International Journal of Solids and Structures 325 (2026) 113696

Contents lists available at ScienceDirect

International Journal of Solids and Structures

journal homepage: www.elsevier.com/locate/ijsolstr

A generalized anisotropic failure criterion for granular materials based on a multi-scale micromechanical approach

Hai-Lin Wang [a,b], Xiaoqiang Gu [a,c,*], Zhen-Yu Yin [b]

[a] Department of Geotechnical Engineering, College of Civil Engineering, Tongji University, Shanghai, China
[b] Department of Civil and Environmental Engineering, The Hong Kong Polytechnic University, Hong Kong, China
[c] School of Civil Engineering and Architecture, Zhejiang Sci-Tech University, Zhejiang, China

ARTICLE INFO

Keywords:
Granular materials
Failure criterion
Fabric anisotropy
Multi-scale
Micromechanics

ABSTRACT

This paper presents an anisotropic failure criterion derived from the relationship between stress and interparticle contact forces within the Chang–Hicher (CH) micromechanical framework. First, we mathematically demonstrate that the failure criterion derived from the CH model for isotropic materials coincides with the Mohr–Coulomb criterion at the critical state. Next, by incorporating the fabric tensor into the Love-Weber formula, we derive strength anisotropy directly at the interparticle scale without additional assumptions. Subsequently, we generalize the anisotropic failure criterion by integrating existing failure criteria through a mobilized friction angle expressed as a function of the Lode angle. The proposed anisotropic criterion, combined with the Von Mises and SMP criteria, is validated using true triaxial test results, demonstrating its effectiveness in predicting the failure behavior of soils under true triaxial conditions with strength anisotropy. Finally, to simulate complex soil behaviors, we adopt an evolution law for fabric anisotropy, and simulation results from hollow cylinder torsional tests validate the proposed model.

1. Introduction

It is well-known that the modeling of failure behavior of soils is one of the most fundamental topics in the field of geotechnical engineering. Various failure criteria have been proposed based on the mechanical behavior of soils with experimental observations. The classical failure criterion, Mohr–Coulomb criterion, which defines a linear relationship between the normal and shear stresses, has been widely used in the field of geotechnical engineering. Hoek and Brown (1980), on the other hand, defined a nonlinear relationship between the maximum and minimum principal stresses under failure state. To consider the effect of the intermediate principal stress ratio under general conditions, Matsuoka and Nakai (1974) introduced the "spatially mobilized plane (SMP)" criterion to capture the smooth dependency of soil behaviors on the Lode angle. Lade and Duncan (1975) proposed a failure criterion in terms of the first and third invariants based on results of true triaxial tests, which has a very similar shape with the SMP criterion in the octahedral plane (denoted as π plane in the following sections). To establish a widely-used failure criterion, Yao et al. (2004) combined the Mises criterion and SMP criterion to form a generalized strength failure criterion.

The aforementioned failure criteria only apply to isotropic materials. In recent years, efforts have been made to consider fabric anisotropy by introducing additional parameters to modify the existing isotropic failure criteria. For example, Mortara (2010) proposed a method in which a scalar function of Lode angle was used to modify the shape of the failure criterion in Mortara (2008). Gao et al. (2010) introduced a fabric anisotropy variable and proposed a nonlinear function to modify the failure criterion based on the generalized strength failure criterion proposed by Yao et al. (2004). Similar work has been done by Wang et al. (2020) for the SMP criterion and Wang et al. (2023) for the Ogawa criterion. Ismael and Konietzky (2019) and Ganesan and Mishra (2024) introduced fabric-dependent material parameters in the Hoek–Brown criterion to consider the effect of fabric anisotropy. Lou and Yoon (2021) introduced anisotropic factors that modifies the DF2016 criterion (Lou and Yoon, 2017) to describe metal behaviors under proportional loading. Lou and Yoon (2021), Sun et al. (2021), Qin et al. (2024a), Huang et al. (2024) and Liu et al. (2024) introduced empirical anisotropic failure criteria for rocks by introducing factors for fabric anisotropy. Pietruszczak and Mroz (2000) proposed a framework to generalize existing isotropic failure criteria to consider the fabric anisotropy with the microstructural fabric tensor. Based on the framework, Lade (2007) proposed a cross-anisotropic failure criterion based on the Lade–Duncan criterion. Xiao et al. (2012) and Kong

* Corresponding author at: Department of Geotechnical Engineering, College of Civil Engineering, Tongji University, Shanghai, China.
E-mail addresses: wanghailin@tongji.edu.cn (H.-L. Wang), guxiaoqiang@tongji.edu.cn (X. Gu), zhenyu.yin@polyu.edu.hk (Z.-Y. Yin).

https://doi.org/10.1016/j.ijsolstr.2025.113696
Received 16 January 2025; Received in revised form 19 August 2025; Accepted 7 October 2025
Available online 20 October 2025

et al. (2013) proposed their cross-anisotropic failure criteria based on the SMP criterion. Furthermore, advanced elastoplastic models have been developed to account for fabric anisotropy, including SANISAND (Taiebat and Dafalias, 2008), SANICLAY (Dafalias et al., 2006), SCLAY1 (Wheeler et al., 2011), ACM (Leoni et al., 2008), and hypoplastic models (Yang et al., 2020; Liao and Yang, 2021b,a). These models typically employ a non-associated plastic flow rule and a kinematic yield surface, incorporating anisotropic parameters into elastoplastic formulations such as the critical state line (Wan and Guo, 2001; Li and Dafalias, 2002; Yang et al., 2020; Liao and Yang, 2021b,a), dilatancy equation and plastic modulus (Dafalias et al., 2004; Dafalias and Manzari, 2004; Li and Dafalias, 2012; Papadimitriou et al., 2019; Petalas et al., 2019), as well as yield and plastic potential functions (Dafalias et al., 2006; Gao et al., 2014; Gao and Zhao, 2017; Gao et al., 2024).

Another frequently used method for considering fabric anisotropy is to introduce a modified stress tensor that transforms the anisotropic materials into equivalent isotropic materials (Tobita, 1988; Karafillis and Boyce, 1993; Pietruszczak and Mroz, 2000). The isotropic failure criteria can then be extended with the modified stress tensor to account for fabric anisotropy. Based on the concept of modified stress tensor, Yao proposed the transformed stress (TS) method (Yao and Wang, 2014) and anisotropic transformed stress (ATS) method (Yao et al., 2017) to generalize existing isotropic failure criteria and constitutive models. Later on, MCC model (Yao and Wang, 2014), UH model (Yao et al., 2017), USC model (Tian and Yao, 2017), SMP criterion (Chen et al., 2020), Lade–Duncan criterion (Dong et al., 2019) have been generalized to consider the fabric anisotropy using the TS and ATS methods. Similarly, Desmorat and Marull (2011) introduced an anisotropic yield criterion based on the Kelvin stress which is a projection of the stress tensor on the Kelvin modes. Lou and Yoon (2017) introduced an anisotropic ductile fracture criterion for metals based on equivalent isotropic damage strain rate tensor. Pei et al. (2018) introduced a normal stress space that incorporates the material structure to consider the fabric anisotropy and the SMP criterion was generalized based on the normal stress space.

Micromechanical models have received more attentions in the last several decades. Taking into account the interparticle contact force–displacement relationship, the macroscopic behavior is derived by averaging interparticle contact forces using the Love-Weber formula (Love, 1927; Weber, 1966). This approach ensures that micromechanical models can effectively capture macroscopic behaviors, similar to the discrete element method (DEM). For example, Hicher and Chang (2007) simulated the behavior of unsaturated soils using the CH micromechanical model (Chang and Hicher, 2005), while Yin et al. (2009) and Chang et al. (2009) applied the same model to simulate the behavior of clay. Bignonnet et al. (2016) proposed a multi-scale micromechanical model to describe the plasticity of porous granular media. Furthermore, by introducing the fabric tensor, micromechanical models can directly account for fabric anisotropy in the summation of contact forces. For instance, Chang and Yin (2010) used the CH micromechanical model to simulate inherent anisotropy by incorporating a non-uniform distribution of friction angles for different contact directions. Similarly, Schweiger et al. (2009) modeled both inherent and induced anisotropies in soils using a multilaminate framework, which inherently captures these anisotropies by integrating macroscopic variables from microscopic ones based on the actual distribution of contact normals. Nguyen and Le (2021) adopted a homogenization approach for failure analysis based on the Tsai–Wu failure criterion. Görthofer et al. (2022) proposed multi-scale model for anisotropic failure of compound composites based on anisotropic damage model on the microscale. Zhao et al. (2023) developed a multi-scale damage method to evaluate anisotropic elastic properties and failure strength for layered rocks. Zhang et al. (2024) proposed an anisotropic stress-dependent failure criterion for heterogeneous reservoirs based on an upscaling numerical method. Yu et al. (2024) proposed an anisotropic damage model to study the localization behavior of brittle materials where the fabric anisotropy is considered by the anisotropic damage multipliers. Although the above studies demonstrate that multi-scale micromechanical models can directly account for fabric anisotropy, a theoretical proof establishing the relationship between microscopic contact forces and the macroscopic failure criterion has not yet been provided.

In this paper, a failure criterion based on the CH micromechanical model was derived. It was assumed that each contact in the micromechanical model represents the stress state on the corresponding plane, and material failure occurs when the first contact fails. This ensures that the CH micromechanical model reduces to the Mohr–Coulomb failure criterion at the critical state on the global scale. By incorporating the fabric tensor into the Love-Weber formula, a closed-form failure criterion accounting for fabric anisotropy was derived which has not been reported previously. This criterion allows for the simulation of soil behaviors without requiring numerical integrations of microscopic quantities, thereby significantly reducing computational costs. Furthermore, the derived failure criterion can be extended to develop elastoplastic models capable of simulating complex soil behaviors. To enhance the generality of the proposed anisotropic failure criterion, a transformation method was introduced to incorporate other isotropic failure criteria to consider fabric anisotropy. For demonstration, the Von Mises, Tresca, and SMP criteria were generalized using the proposed method. The proposed anisotropic failure criterion was validated by true triaxial test results. The results indicate that the proposed failure criterion effectively predicts the failure behavior of soils under true triaxial conditions.

2. Revisit the CH micromechanical model

The CH micromechanical model was initially proposed by Chang and Hicher (2005) for sands. It was then extended to simulate unsaturated soils (Hicher and Chang, 2007; Zhao et al., 2017) and clays (Chang et al., 2009; Yin et al., 2014). The framework of the CH micromechanical model shown in Fig. 1 consists of 4 steps: (1) localization; (2) contact law integration; (3) averaging; (4) unbalanced force checking.

Firstly, the global stress is localized to the contact force based on the static hypothesis:

$$f_i = \sigma_{ij} A_{jn} l_n \tag{1}$$

where f_i is the contact force, σ_{ij} is the stress tensor, l_n is the branch vector, A_{jn} is a fabric tensor defined as:

$$A_{jn} = \left(\frac{1}{V} \sum_{c=1}^{N} l_j^c l_n^c \right)^{-1} \tag{2}$$

where V is the volume of the representative element, N is the number of contacts. According to the definition, the second-order deviatoric fabric tensor F_{jn} can be related to the fabric tensor A_{jn} by the following equation:

$$\left(A_{jn}\right)^{-1} = \frac{1}{V} \sum_{c=1}^{N} l_j^c l_n^c = 4r^2 \frac{N}{V} N_{jn} = 4r^2 \frac{N}{V} \left(\frac{2}{15} F_{jn} + \frac{1}{3} I_{jn} \right) \tag{3}$$

where r is the particle radius, I_{jn} is an identity matrix. Then, the local contact law is employed to update the contact force:

$$\mathrm{d}f_i = k_{ij} \mathrm{d}u_j \tag{4}$$

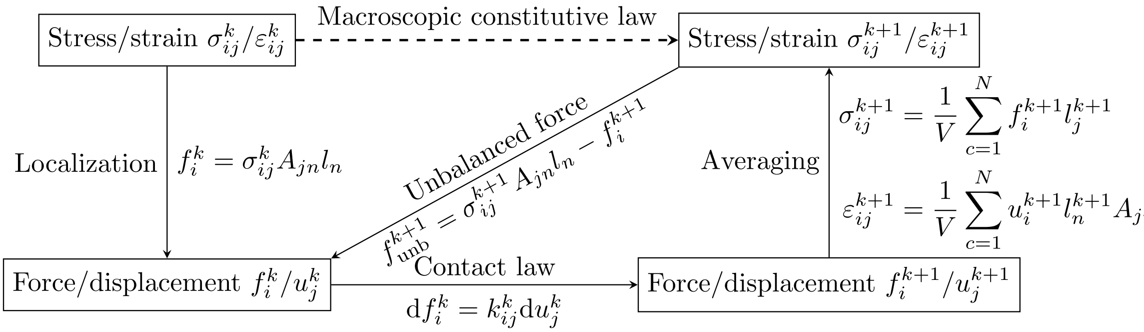

Fig. 1. Framework of the CH micromechanical model.

Table 1
Formulations of contact law in the CH micromechanical model.

Category	Equation
Elasticity	$k_n = k_{n0}\left(\frac{f_n}{f_{ref}}\right)^{n_e}, k_r = k_{rR}$
Yield surface	$F = f_r^c - f_n^c \frac{k_p^c \tan\phi_p u_r^{p,c}}{f_n^c \tan\phi_p + k_p^c u_r^{p,c}}, k_p^c = k_{pR} k_n^c, \tan\phi_p = \left(\frac{e_c}{e}\right)^{n_p}\tan\phi$
Flow rule	$D = \frac{\mathrm{d}u_n^{p,c}}{\mathrm{d}u_r^{p,c}} = A_d\left(\tan\phi_d - \frac{f_r^c}{f_n^c}\right), \tan\phi_d = \left(\frac{e}{e_c}\right)^{n_d}\tan\phi$
Critical state line	$e_c = e_{ref} - \lambda\left(\frac{p'}{p_a}\right)^{\xi}$

where $k_{ij} = \mathrm{diag}([k_n, k_r, k_r])$ is the contact stiffness matrix. Table 1 shows the formulations of the contact law used in the CH micromechanical model. Detailed description of the contact law can be found in Chang and Hicher (2005) and will not be repeated here.

The relationship between the local contact force and the global stress is given by the Love-Weber formula (Love, 1927; Weber, 1966):

$$\sigma_{ij} = \frac{1}{V}\sum_{c=1}^{N} f_i^c l_j^c \tag{5}$$

After that, the local forces are checked to ensure it is balanced with the global stress.

It should be noted that transforming between global stress and strain and local force and displacement requires a coordinate system transformation. As illustrated in Fig. 2, the local (n, s, t) and global (x_1, x_2, x_3) coordinate systems are defined as follows: the azimuthal angle γ denotes the angle between the contact normal and the x_1-axis, while β represents the angle between the projection of the contact normal onto the x_2x_3 plane and the x_2-axis. The directions n, s, and t correspond to the directions of increasing r, γ, and β, respectively. According to Iyanaga and Kawada (1993), any local quantity ($\mathbf{Q}_{\text{local}}$) can be transformed into global coordinates ($\mathbf{Q}_{\text{global}}$) using the following rotation matrix:

$$\begin{gathered}\mathbf{Q}_{\text{local}} = \mathbf{R}\mathbf{Q}_{\text{global}}, \mathbf{Q}_{\text{global}} = \mathbf{R}^{-1}\mathbf{Q}_{\text{local}} = \mathbf{R}^{\mathrm{T}}\mathbf{Q}_{\text{local}} \\ \mathbf{R} = \begin{bmatrix} \cos\gamma & \sin\gamma\cos\beta & \sin\gamma\sin\beta \\ -\sin\gamma & \cos\gamma\cos\beta & \cos\gamma\sin\beta \\ 0 & -\sin\beta & \cos\beta \end{bmatrix}\end{gathered} \tag{6}$$

3. Derivation of the anisotropic failure criterion

In this section, an explicit anisotropic failure criterion is derived based on the static hypothesis in Eq. (1) and the Love-Weber formula in Eq. (5).

3.1. Conventional triaxial conditions

Under conventional triaxial conditions, the stress in the micromechanical model calculated by Eq. (5) can be simplified as:

$$\boldsymbol{\sigma} = \frac{2r}{V}\sum_{c=1}^{N}\begin{bmatrix} \cos\gamma & -\sin\gamma & 0 \\ \sin\gamma\cos\beta & \cos\gamma\cos\beta & -\sin\beta \\ \sin\gamma\sin\beta & \cos\gamma\sin\beta & \cos\beta \end{bmatrix}\begin{bmatrix} f_n \\ f_s \\ f_t \end{bmatrix}\begin{bmatrix} \cos\gamma \\ \sin\gamma\cos\beta \\ \sin\gamma\sin\beta \end{bmatrix}^{\mathrm{T}} \tag{7}$$

Note that the superscript c is omitted for contact variables in the following discussion for simplicity. Under conventional triaxial conditions, the principal stresses can be further simplified as follow:

$$\begin{aligned}\sigma_1 &= \frac{2r}{V}\sum_{c=1}^{N}\left(f_n\cos^2\gamma - f_s\sin\gamma\cos\gamma\right) \\ \sigma_2 &= \frac{2r}{V}\sum_{c=1}^{N}\left(f_n\sin^2\gamma\cos^2\beta + f_s\sin\gamma\cos\gamma\cos^2\beta - f_t\sin\gamma\sin\beta\cos\beta\right) \\ \sigma_3 &= \frac{2r}{V}\sum_{c=1}^{N}\left(f_n\sin^2\gamma\sin^2\beta + f_s\sin\gamma\cos\gamma\sin^2\beta + f_t\sin\gamma\sin\beta\cos\beta\right)\end{aligned} \tag{8}$$

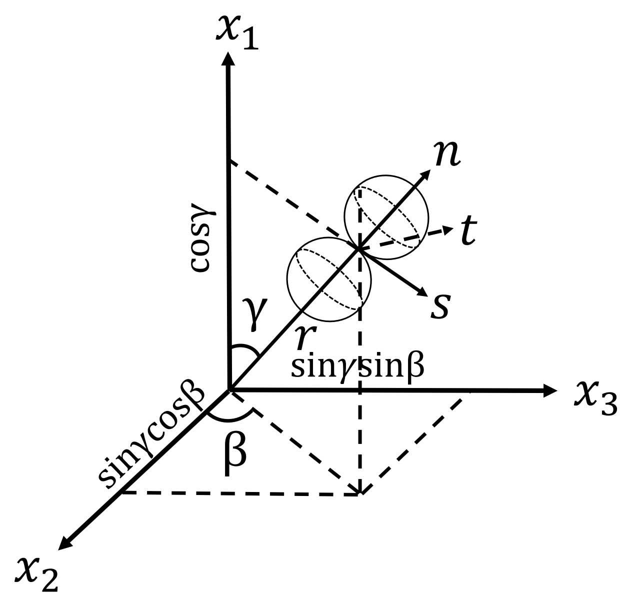

Fig. 2. Local and global coordinate systems.

where σ_1, σ_2, and σ_3 are the principal stresses, f_n, f_s, and f_t are the normal contact force and shear contact forces in two directions, respectively. The mean and deviatoric stresses can be calculated as:

$$\begin{aligned} p &= \frac{1}{3}\mathrm{tr}(\boldsymbol{\sigma}) = \frac{2r}{3V}\sum_{c=1}^{N} f_n \\ q &= \sqrt{3J_2} = \frac{1}{2}\left|2\sigma_1 - (\sigma_2+\sigma_3)\right| = \frac{r}{V}\sum_{c=1}^{N}\left|2f_n - 3\left(f_n\sin^2\gamma + f_s\sin\gamma\cos\gamma\right)\right| \end{aligned} \tag{9}$$

where p is the mean stress, q is the deviatoric stress and J_2 is the second invariant of the deviatoric stress tensor. Based on the static hypothesis shown in Eq. (1), the contact force in the micromechanical model can be calculated as:

$$\mathbf{f} = \frac{V}{2rN}\begin{bmatrix} \cos\gamma & \sin\gamma\cos\beta & \sin\gamma\sin\beta \\ -\sin\gamma & \cos\gamma\cos\beta & \cos\gamma\sin\beta \\ 0 & -\sin\beta & \cos\beta \end{bmatrix}\begin{bmatrix} \sigma_{11} & \tau_{12} & \tau_{13} \\ \tau_{12} & \sigma_{22} & \tau_{23} \\ \tau_{13} & \tau_{23} & \sigma_{33} \end{bmatrix}\left(\frac{2}{15}\mathbf{F} + \frac{1}{3}\mathbf{I}\right)^{-1}\begin{bmatrix} \cos\gamma \\ \sin\gamma\cos\beta \\ \sin\gamma\sin\beta \end{bmatrix} \tag{10}$$

For isotropic materials under conventional triaxial conditions, the normal and shear contact forces can be simplified as:

$$\begin{aligned} f_n &= -\frac{3V}{2rN}\left(\sigma_1\cos^2\gamma + \sigma_2\sin^2\gamma\cos^2\beta + \sigma_3\sin^2\gamma\sin^2\beta\right) \\ f_s &= \frac{3V}{2rN}\left(\sigma_1\sin\gamma\cos\gamma - \sigma_2\cos\gamma\cos\beta\sin\gamma\cos\beta - \sigma_3\cos\gamma\sin\beta\sin\gamma\sin\beta\right) \\ f_t &= \frac{3V}{2rN}\left(\sigma_2\sin\beta\sin\gamma\cos\beta - \sigma_3\cos\beta\sin\gamma\sin\beta\right) \end{aligned} \tag{11}$$

It should be noted that compression forces are considered positive; therefore, a negative sign is used in the normal force. Under the conventional triaxial stress conditions, $\sigma_2 = \sigma_3$, the contact forces can be further simplified as:

$$\begin{aligned} f_n &= -\frac{3V}{2rN}\left(\sigma_1\cos^2\gamma + \sigma_3\sin^2\gamma\right) = -\frac{3V}{2rN}\left(\frac{\sigma_1+\sigma_3}{2} + \frac{\sigma_1-\sigma_3}{2}\cos 2\gamma\right) \\ f_s &= \frac{3V}{2rN}\left(\sigma_1\sin\gamma\cos\gamma - \sigma_3\sin\gamma\cos\gamma\right) = \frac{3V}{2rN}\left(\frac{\sigma_1-\sigma_3}{2}\sin 2\gamma\right) \\ f_t &= 0 \end{aligned} \tag{12}$$

It is clear that the normal and shear forces can be expressed as:

$$\begin{aligned} f_n &= -\left(f_{n13} + R_{13}\cos 2\gamma\right) \\ f_s &= R_{13}\sin 2\gamma \end{aligned} \tag{13}$$

where R_{13} and f_{n13} are defined as:

$$\begin{aligned} R_{13} &= \frac{3V}{4rN}\left(\sigma_1 - \sigma_3\right) \\ f_{n13} &= \frac{3V}{4rN}\left(\sigma_1 + \sigma_3\right) \end{aligned} \tag{14}$$

Eq. (14) shows that the normal and shear forces in Eq. (13) lie on a circle with the center at $(f_{n13}, 0)$ and a radius of R_{13}. For further demonstration, drained and undrained triaxial tests are simulated using the CH model with the parameters in Table 2. The evolution of the contact forces under drained and undrained conditions is presented in Fig. 3. As observed, under both drained and undrained conditions, the contact normal and shear

Table 2
Model parameters for the CH micromechanical model.

k_{n0} (N/mm)	n_e	k_{rR}	k_{pR}	ϕ_c (°)	e_{ref}	λ	ξ	n_p	n_d	A_d
80	0.5	0.4	0.4	33	0.81	0.06	1	2	4	0.6

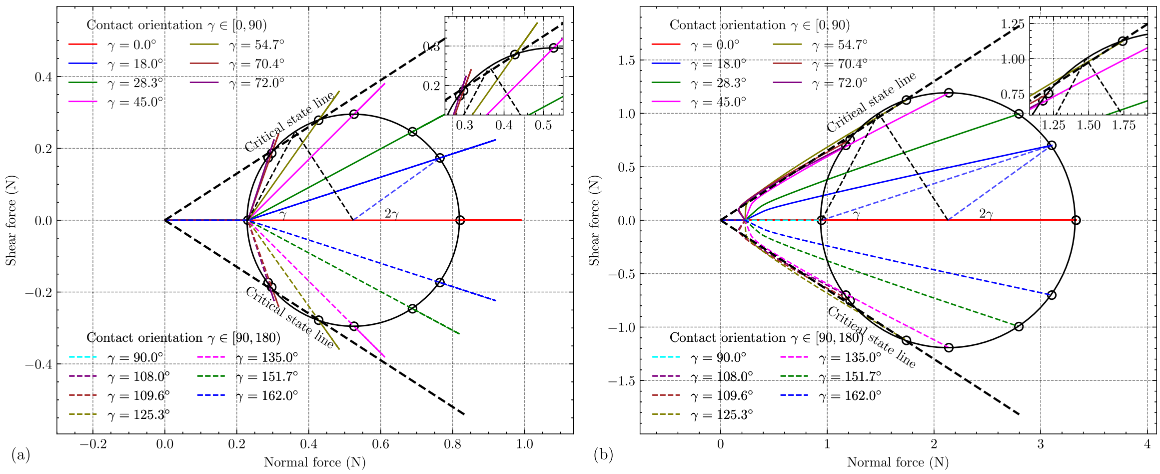

Fig. 3. Evolution of contact forces: (a) drained triaxial tests; (b) undrained triaxial tests.

forces consistently lie on a circle, which closely resembles Mohr's circle in macroscopic stress space. This indicates that each contact represents the stress state in that direction. These findings suggest that the CH model effectively describes the relationship between shear stress and normal stress in various directions at the contact level, aligning with the Mohr–Coulomb criterion.

Now, we can derive the critical stress ratio based on the Mohr's circle. Substituting Eq. (13) into Eq. (9), the mean and deviatoric stresses can be expressed as:

$$\begin{aligned} p &= \frac{2r}{3V}\sum_{c=1}^{N} f_n = \frac{2r}{3V}\sum_{c=1}^{N}\left(f_{n13} + R_{13}\cos 2\gamma\right) = \frac{2rN}{3V}\left(f_{n13} + \frac{R_{13}}{N}\sum_{c=1}^{N}\cos 2\gamma\right) \\ q &= \frac{r}{V}\sum_{c=1}^{N}\left|2f_n - 3\left(f_n\sin^2\gamma + f_s\sin\gamma\cos\gamma\right)\right| \\ &= \frac{rN}{V}\left|-2f_{n13} - \frac{2R_{13}}{N}\sum_{c=1}^{N}\cos 2\gamma + \frac{3f_{n13}}{N}\sum_{c=1}^{N}\sin^2\gamma + \frac{3R_{13}}{N}\sum_{c=1}^{N}\cos 2\gamma\sin^2\gamma - \frac{3R_{13}}{2N}\sum_{c=1}^{N}\sin^2 2\gamma\right| \end{aligned} \tag{15}$$

For isotropic materials, the summations in Eq. (15) can be calculated as:

$$\begin{aligned} &\frac{1}{N}\sum_{c=1}^{N}\cos 2\gamma = \frac{1}{4\pi}\int_0^{2\pi}\int_0^{\pi}\cos 2\gamma\cdot\sin\gamma\, d\gamma\, d\beta = -\frac{1}{3} \\ &\frac{1}{N}\sum_{c=1}^{N}\sin^2\gamma = \frac{2}{3},\ \frac{1}{N}\sum_{c=1}^{N}\cos 2\gamma\sin^2\gamma = -\frac{2}{5},\ \frac{1}{N}\sum_{c=1}^{N}\sin^2 2\gamma = \frac{8}{15} \end{aligned} \tag{16}$$

Substituting Eq. (16) into Eq. (15), the mean and deviatoric stresses can be calculated as:

$$\begin{aligned} p &= \frac{2rN}{3V}\left(f_{n13} - \frac{R_{13}}{3}\right) \\ q &= \frac{rN}{V}\left|-2f_{n13} + \frac{2R_{13}}{3} + 2f_{n13} - \frac{6R_{13}}{5} - \frac{4R_{13}}{5}\right| = \frac{rN}{V}\frac{4|R_{13}|}{3} \end{aligned} \tag{17}$$

Then, the stress ratio can be calculated as:

$$\eta = \frac{q}{p} = \frac{\dfrac{rN}{V}\dfrac{4|R_{13}|}{3}}{\dfrac{2rN}{3V}\left(f_{n13} - \dfrac{R_{13}}{3}\right)} = \frac{\dfrac{2rN}{9V}\cdot 6|R_{13}|}{\dfrac{2rN}{9V}\left(3f_{n13} - R_{13}\right)} = \frac{6|R_{13}|}{3f_{n13} - R_{13}} \tag{18}$$

According to Fig. 3, for critical state, $R_{13} = \pm f_{n13}\sin\phi$ (positive for triaxial compression (TC) and negative for triaxial extension (TE)). Therefore, the stress ratio at the critical state can be simplified as:

$$M = \frac{6f_{n13}\sin\phi}{3f_{n13} \mp f_{n13}\sin\phi} = \frac{6\sin\phi}{3 \mp \sin\phi} \tag{19}$$

3.2. True triaxial conditions

Under true triaxial conditions and assuming $\sigma_1 \geq \sigma_2 \geq \sigma_3$, the mean and deviatoric stresses can be calculated as:

$$p = \frac{1}{3}\mathrm{tr}\,(\boldsymbol{\sigma}) = \frac{2r}{3V}\sum_{c=1}^{N} f_n$$
$$q = \sqrt{3J_2} = \frac{\sqrt{b^2-b+1}}{2-b}\cdot\left|2\sigma_1 - \left(\sigma_2+\sigma_3\right)\right| = \frac{rh(b)}{V}\sum_{c=1}^{N}\left|2f_n - 3\left(f_n\sin^2\gamma + f_s\sin\gamma\cos\gamma\right)\right| \tag{20}$$

where $b = (\sigma_2-\sigma_3)/(\sigma_1-\sigma_3)$ is the intermediate principal stress ratio and $h(b)$ is defined as:

$$h(b) = \frac{2\sqrt{b^2-b+1}}{2-b} \tag{21}$$

The contact forces shown in Eq. (11) should be revised as:

$$f_n = -\frac{3V}{2rN}\left[\frac{\sigma_1+\sigma_2}{4} + \frac{\sigma_1-\sigma_2}{4}\cos 2\gamma + \frac{\sigma_1+\sigma_3}{4} + \frac{\sigma_1-\sigma_3}{4}\cos 2\gamma + \frac{\sigma_2-\sigma_3}{2}\sin^2\gamma\cos 2\beta\right]$$
$$f_s = \frac{3V}{2rN}\left[\frac{\sigma_1-\sigma_2}{4}\sin 2\gamma + \frac{\sigma_1-\sigma_3}{4}\sin 2\gamma - \frac{\sigma_2-\sigma_3}{2}\sin\gamma\cos\gamma\cos 2\beta\right] \tag{22}$$
$$f_t = \frac{3V}{2rN}\left(\frac{\sigma_2-\sigma_3}{2}\sin\gamma\sin 2\beta\right)$$

Let f_{n23}, f_{s23}, and f_{t23} be the forces contributed by the $\sigma_2-\sigma_3$ terms in Eq. (22):

$$f_{n23} = -\frac{3V}{2rN}\left(\frac{\sigma_2-\sigma_3}{2}\sin^2\gamma\cos 2\beta\right) = -bR_{13}\sin^2\gamma\cos 2\beta$$
$$f_{s23} = -\frac{3V}{2rN}\left(\frac{\sigma_2-\sigma_3}{2}\sin\gamma\cos\gamma\cos 2\beta\right) = -bR_{13}\sin\gamma\cos\gamma\cos 2\beta \tag{23}$$
$$f_{t23} = \frac{3V}{2rN}\left(\frac{\sigma_2-\sigma_3}{2}\sin\gamma\sin 2\beta\right) = bR_{13}\sin\gamma\sin 2\beta$$

Substituting Eq. (23) into Eq. (20), the mean and deviatoric stresses contributed by the $\sigma_2-\sigma_3$ terms can be calculated as:

$$p_1 = \frac{2r}{3V}\sum_{c=1}^{N} f_n = \frac{2rbR_{13}N}{3V}\frac{1}{N}\sum_{c=1}^{N}\sin^2\gamma\cos 2\beta$$
$$q_1 = \frac{rh(b)}{V}\sum_{c=1}^{N}\left|2f_n - 3\left(f_n\sin^2\gamma + f_s\sin\gamma\cos\gamma\right)\right| \tag{24}$$
$$= \frac{rh(b)bR_{13}N}{V}\left|-\frac{2}{N}\sum_{c=1}^{N}\sin^2\gamma\cos 2\beta + \frac{3}{N}\sum_{c=1}^{N}\sin^4\gamma\cos 2\beta + \frac{3}{N}\sum_{c=1}^{N}\sin^2\gamma\cos^2\gamma\cos 2\beta\right|$$

It is found out that the summations in Eq. (24) under isotropic conditions are all zeros:

$$\frac{1}{N}\sum_{c=1}^{N}\sin^2\gamma\cos 2\beta = \frac{1}{4\pi}\int_0^{2\pi}\int_0^{\pi}\sin^2\gamma\cos 2\beta\cdot\sin\gamma\mathrm{d}\gamma\mathrm{d}\beta = 0$$
$$\frac{1}{N}\sum_{c=1}^{N}\sin^4\gamma\cos 2\beta = 0,\ \frac{1}{N}\sum_{c=1}^{N}\sin^2\gamma\cos^2\gamma\cos 2\beta = 0 \tag{25}$$

Eq. (25) indicates that the $\sigma_2-\sigma_3$ terms in Eq. (22) does not contribute to the mean and deviatoric stresses. Therefore, according to Eq. (20), Eq. (22) and the solution where the conventional triaxial conditions are assumed, the stress ratio under true triaxial conditions can be calculated as:

$$\eta = h(b)\cdot\frac{\left|6R_{12,13}\right|}{3f_{n12,13} - R_{12,13}} \tag{26}$$

where $f_{n12,13}$ is the average of f_{n12} and f_{n13}, and $R_{12,13}$ is the average of R_{12} and R_{13}. At the critical state, $f_{n12,13}$ and $R_{12,13}$ can be calculated as:

$$f_{n12,13} = \frac{f_{n12}+f_{n13}}{2} = \frac{f_{n13}+bR_{13}+f_{n13}}{2} = \frac{2+b\sin\phi}{2}f_{n13}$$
$$R_{12,13} = \frac{R_{12}+R_{13}}{2} = \frac{(1-b)R_{13}+R_{13}}{2} = \frac{2-b}{2}f_{n13}\sin\phi \tag{27}$$

Therefore, Eq. (26) can be simplified as:

$$M = h(b)\cdot\frac{\left|6\cdot\frac{2-b}{2}f_{n13}\sin\phi\right|}{3\cdot\frac{2+b\sin\phi}{2}f_{n13} - \frac{2-b}{2}f_{n13}\sin\phi} = \frac{6\sqrt{b^2-b+1}\sin\phi}{3+(2b-1)\sin\phi} \tag{28}$$

Eq. (28) represents the critical stress ratio of the Mohr–Coulomb criterion for different Lode angles. Substituting $b = (\sigma_2-\sigma_3)/(\sigma_1-\sigma_3)$ into Eq. (28) leads to:

$$\sin\phi = \frac{\sigma_1-\sigma_3}{\sigma_1+\sigma_3} \tag{29}$$

Fig. 4 shows the evolution of local forces under true triaxial conditions with different number of integration points. As seen in Fig. 4, under true triaxial conditions, the failure line does not remain tangent to the Mohr's circle, resulting in larger error compared to conventional triaxial conditions. However, increasing the number of integration points significantly reduces this error.

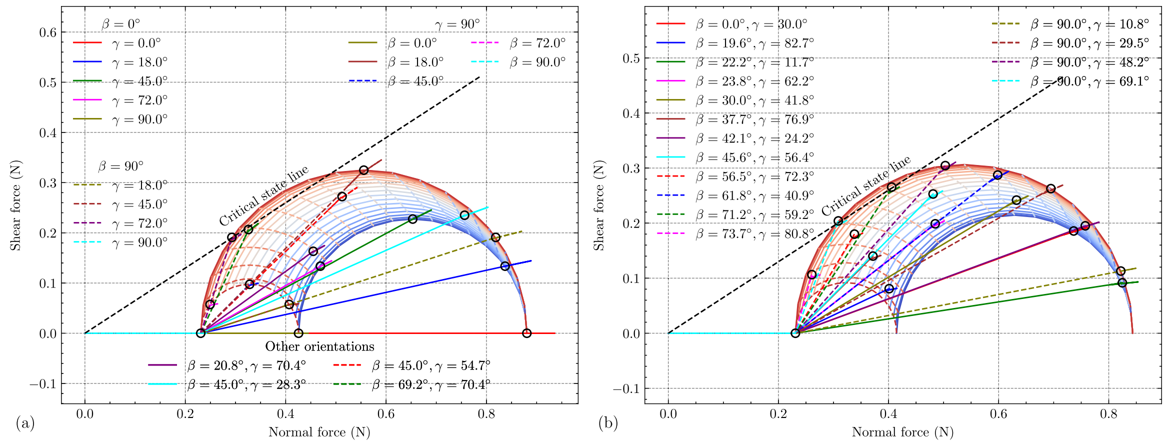

Fig. 4. Evolution of contact forces under true triaxial conditions with different integration points: (a) 74 points; (b) 122 points.

3.3. Anisotropic conditions

Under anisotropic conditions, the fabric tensor $\mathbf{A}$ in Eq. (1) is no longer a diagonal matrix with three equal principal values. Defining the following modified stress tensor:

$$\boldsymbol{\sigma}' = \boldsymbol{\sigma}\mathbf{A}\left(\mathbf{A}^{\mathrm{iso}}\right)^{-1} = \boldsymbol{\sigma}\left(\mathbf{I} + \frac{2}{5}\mathbf{F}\right)^{-1} \tag{30}$$

Then, the modified stress tensor $\boldsymbol{\sigma}'$ can be triangularized as:

$$\boldsymbol{\sigma}' = \mathbf{P}\begin{bmatrix} \sigma_1' & 0 & 0 \\ 0 & \sigma_2' & 0 \\ 0 & 0 & \sigma_3' \end{bmatrix}\mathbf{P}^{-1} \tag{31}$$

where $\mathbf{P}$ is the similarity transformation matrix, and $\sigma_1' \geq \sigma_2' \geq \sigma_3'$ are the principal stresses of the modified stress tensor. The original stress tensor $\boldsymbol{\sigma}$ and second-order deviatoric fabric tensor $\mathbf{F}$ can be transformed in the modified stress space:

$$\begin{aligned} \widetilde{\boldsymbol{\sigma}} &= \mathbf{P}^{-1}\boldsymbol{\sigma}\mathbf{P} \\ \widetilde{\mathbf{F}} &= \mathbf{P}^{-1}\mathbf{F}\mathbf{P} \end{aligned} \tag{32}$$

Based on the modified stress tensor, Eq. (1) can be simplified as:

$$f_i = \sigma_{ij}A_{jn}l_n = \sigma_{ij}'A_{jn}^{\mathrm{iso}}l_n \tag{33}$$

Eq. (33) shows that with the modified stress tensor, the contact force can be calculated just like the material is isotropic. In fact, the modified stress tensor shown in Eq. (30) is very much like the modified stress tensor proposed by Tobita (1988) which has been used as a basis for the TS and ATS methods to generalize isotropic failure criteria. Assuming f_n', f_s', and f_t' are contact forces corresponding to the modified stress tensor, the mean and deviatoric stresses should be calculated as:

$$\begin{aligned} p &= \frac{2r}{3V}\sum_{c=1}^{N} f_n' \\ q &= \frac{rh(\widetilde{b})}{V}\sum_{c=1}^{N}\left|2f_n' - 3\left(f_n'\sin^2\gamma + f_s'\sin\gamma\cos\gamma\right)\right| \end{aligned} \tag{34}$$

where $\widetilde{b} = (\widetilde{\sigma}_{22} - \widetilde{\sigma}_{33}) / (\widetilde{\sigma}_{11} - \widetilde{\sigma}_{33})$ is the modified intermediate principal stress ratio defined by the stress tensor $\widetilde{\sigma}_{ij}$ shown in Eq. (32). The contact forces f_n', f_s', and f_t' are defined as:

$$\begin{aligned} f_n' &= -\frac{3V}{2rN}\left[\frac{\sigma_1' + \sigma_2'}{4} + \frac{\sigma_1' - \sigma_2'}{4}\cos 2\gamma + \frac{\sigma_1' + \sigma_3'}{4} + \frac{\sigma_1' - \sigma_3'}{4}\cos 2\gamma + \frac{\sigma_2' - \sigma_3'}{2}\sin^2\gamma\cos 2\beta\right] \\ f_s' &= \frac{3V}{2rN}\left[\frac{\sigma_1' - \sigma_2'}{4}\sin 2\gamma + \frac{\sigma_1' - \sigma_3'}{4}\sin 2\gamma - \frac{\sigma_2' - \sigma_3'}{2}\sin\gamma\cos\gamma\cos 2\beta\right] \\ f_t' &= \frac{3V}{2rN}\left(\frac{\sigma_2' - \sigma_3'}{2}\sin\gamma\sin 2\beta\right) \end{aligned} \tag{35}$$

Similar to Eq. (24) for isotropic materials, the mean and deviatoric stresses contributed by the $\sigma_2' - \sigma_3'$ terms can be calculated as:

$$\begin{aligned} p_1 &= \frac{2r}{3V}\sum_{c=1}^{N} f_n' = \frac{2rb'R_{13}'N}{3V}\frac{1}{N}\sum_{c=1}^{N}\sin^2\gamma\cos 2\beta \\ q_1 &= \frac{rh(\widetilde{b})b'R_{13}'N}{V}\left|-\frac{2}{N}\sum_{c=1}^{N}\sin^2\gamma\cos 2\beta + \frac{3}{N}\sum_{c=1}^{N}\sin^4\gamma\cos 2\beta + \frac{3}{N}\sum_{c=1}^{N}\sin^2\gamma\cos^2\gamma\cos 2\beta\right| \end{aligned} \tag{36}$$

where b' and R'_{13} are the intermediate principal stress ratio and radius of the Mohr's circle corresponding to the major and minor principal stresses under the modified stress tensor space. In the following, f'_{n12}, f'_{n13}, and R'_{12} will also be used as the corresponding values under the original stress tensor space. For anisotropic materials, the summations in Eq. (36) can be calculated as:

$$\begin{aligned}&\frac{1}{N}\sum_{c=1}^{N}\sin^2\gamma\cos 2\beta=\int_0^{2\pi}\int_0^{\pi}\sin^2\gamma\cos 2\beta\cdot\xi(\gamma,\beta)\cdot\sin\gamma\mathrm{d}\gamma\mathrm{d}\beta=\frac{2}{15}\left(\widetilde{F}_{22}-\widetilde{F}_{33}\right)\\&\frac{1}{N}\sum_{c=1}^{N}\sin^4\gamma\cos 2\beta=\frac{4}{35}\left(\widetilde{F}_{22}-\widetilde{F}_{33}\right),\ \frac{1}{N}\sum_{c=1}^{N}\sin^2\gamma\cos^2\gamma\cos 2\beta=\frac{2}{105}\left(\widetilde{F}_{22}-\widetilde{F}_{33}\right)\end{aligned}\tag{37}$$

where $\xi(\gamma,\beta)$ is density function of the contact normal distribution which is defined as:

$$\xi(\gamma,\beta)=\frac{1}{4\pi}\left(1+\widetilde{F}_{jn}n_jn_n\right)\tag{38}$$

where $n_j=n_n=\begin{bmatrix}\cos\gamma & \sin\gamma\cos\beta & \sin\gamma\sin\beta\end{bmatrix}^{\mathrm{T}}$ is an unit direction vector of the contact normal. Therefore, the mean and deviatoric stresses in Eq. (36) can be calculated as:

$$\begin{aligned}p_1&=\frac{2rb'R'_{13}N}{3V}\frac{1}{N}\sum_{c=1}^{N}\sin^2\gamma\cos 2\beta=\frac{2rb'R'_{13}N}{3V}\cdot\frac{2}{15}\left(\widetilde{F}_{22}-\widetilde{F}_{33}\right)=\frac{4rb'R'_{13}N\left(\widetilde{F}_{11}+2\widetilde{F}_{22}\right)}{45V}\\q_1&=\frac{rh(\widetilde{b})b'R'_{13}N}{V}\left|-\frac{2}{N}\sum_{c=1}^{N}\sin^2\gamma\cos 2\beta+\frac{3}{N}\sum_{c=1}^{N}\sin^4\gamma\cos 2\beta+\frac{3}{N}\sum_{c=1}^{N}\sin^2\gamma\cos^2\gamma\cos 2\beta\right|\\&=\frac{2rh(\widetilde{b})b'R'_{13}N\left|\widetilde{F}_{11}+2\widetilde{F}_{22}\right|}{15V}\end{aligned}\tag{39}$$

For anisotropic materials, summations in Eq. (16) can be calculated as:

$$\begin{aligned}&\frac{1}{N}\sum_{c=1}^{N}\cos 2\gamma=\frac{4}{15}\widetilde{F}_{11}-\frac{1}{3},\ \frac{1}{N}\sum_{c=1}^{N}\sin^2\gamma=-\frac{2}{15}\widetilde{F}_{11}+\frac{2}{3}\\&\frac{1}{N}\sum_{c=1}^{N}\cos 2\gamma\sin^2\gamma=\frac{6}{35}\widetilde{F}_{11}-\frac{2}{5},\ \frac{1}{N}\sum_{c=1}^{N}\sin 2\gamma\sin\gamma\cos\gamma=\frac{4}{105}\widetilde{F}_{11}+\frac{4}{15}\end{aligned}\tag{40}$$

The mean and deviatoric stresses under conventional triaxial conditions can be calculated as:

$$\begin{aligned}p&=\frac{2rN}{3V}\left[f_{n13}+R_{13}\left(\frac{4}{15}\widetilde{F}_{11}-\frac{1}{3}\right)\right]\\q&=\frac{rN}{V}\left|-\frac{2}{5}\widetilde{F}_{11}f_{n13}-\left(\frac{2}{15}\widetilde{F}_{11}+\frac{4}{3}\right)R_{13}\right|\end{aligned}\tag{41}$$

Therefore, the stress ratio under true triaxial conditions can be calculated as:

$$\eta=\frac{q}{p}=h(\widetilde{b})\cdot\frac{\frac{rN}{V}\left|-\frac{2}{5}\widetilde{F}_{11}f'_{n12,13}-\left(\frac{2}{15}\widetilde{F}_{11}+\frac{4}{3}\right)R'_{12,13}+\frac{2}{15}b'R'_{13}\left(\widetilde{F}_{11}+2\widetilde{F}_{22}\right)\right|}{\frac{2rN}{3V}\left[f'_{n12,13}+R'_{12,13}\left(\frac{4}{15}\widetilde{F}_{11}-\frac{1}{3}\right)+\frac{2}{15}b'R'_{13}\left(\widetilde{F}_{11}+2\widetilde{F}_{22}\right)\right]}\tag{42}$$

where $f'_{n12,13}$ is the average of f'_{n12} and f'_{n13}, and $R'_{12,13}$ is the average of R'_{12} and R'_{13}. At critical state, $f'_{n12,13}$ and $R'_{12,13}$ can be calculated as:

$$\begin{aligned}f'_{n12,13}&=\frac{f'_{n12}+f'_{n13}}{2}=\frac{f'_{n13}+b'R'_{13}+f'_{n13}}{2}=\frac{2+b'\sin\phi}{2}f'_{n13}\\R'_{12,13}&=\frac{R'_{12}+R'_{13}}{2}=\frac{(1-b')R'_{13}+R'_{13}}{2}=\frac{2-b'}{2}f'_{n13}\sin\phi\end{aligned}\tag{43}$$

Substituting Eq. (43) into Eq. (42) leads to:

$$M=\frac{6\sqrt{\widetilde{b}^2-\widetilde{b}+1}}{2-\widetilde{b}}\frac{\left(2+\frac{1}{5}\widetilde{F}_{11}\right)\sin\phi-\left(1+\frac{2}{5}\widetilde{F}_{22}\right)b'\sin\phi+\frac{3}{5}\widetilde{F}_{11}}{3+\left[2\left(1+\frac{2}{5}\widetilde{F}_{22}\right)b'-\left(1-\frac{4}{5}\widetilde{F}_{11}\right)\right]\sin\phi}\tag{44}$$

To this end, a failure criterion accounting for fabric anisotropy has been derived based on the CH micromechanical model.

3.4. Integration of other failure criteria

The above analysis demonstrates that the proposed anisotropic failure criterion reduces to the Mohr–Coulomb criterion at critical state when a Coulomb-type interparticle contact law is employed. The key difference lies in the ability of the micromechanics-based failure criterion proposed herein to account for material anisotropy, whereas the classical Mohr–Coulomb criterion lacks this capability. Moreover, the Mohr–Coulomb criterion suffers from an unsmooth failure envelope in the π plane and its inability to account for the intermediate principal stress (Li et al., 2024). Experimental studies (Haruyama, 1981; Ochiai and Lade, 1983; Lam and Tatsuoka, 1988; Kirkgard and Lade, 1993; Abelev and Lade, 2004) also showed that the friction angle varies with the Lode angle rather than remaining constant as is often assumed. Considering that the Mohr–Coulomb criterion has been widely applied in geotechnical engineering, particularly in slope stability analysis, footing bearing capacity assessment, pile driving and tunneling. Consequently, developing a method to transform existing failure criteria to the Mohr–Coulomb criterion would be beneficial.

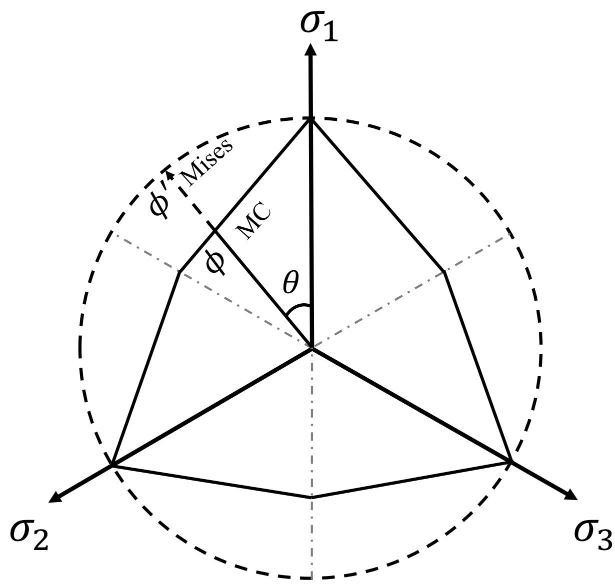

Fig. 5. Transformation of the Mohr–Coulomb criterion to Von Mises criterion.

To achieve this, a mobilized friction angle that depends on the Lode angle is introduced in the anisotropic failure criterion. As shown in Fig. 5, the failure envelope in the π plane can be transformed into any desired shapes by using a mobilized friction angle. This transformation is similar to the TS method (Yao and Wang, 2014), which transforms any failure criteria to the Von Mises criterion instead of the Mohr–Coulomb criterion based on a modified stress tensor. Regarding the loading direction, the anisotropic failure criterion presented in Eq. (44) already accounts for fabric anisotropy, and no additional considerations are required.

3.4.1. Von Mises criterion

By maintaining a constant stress ratio for different Lode angles, a failure criterion similar to the Von Mises criterion can be incorporated into the anisotropic failure criterion. However, it is represented by a conical surface rather than a cylindrical one in the principal stress space. The mobilized friction angle ϕ_{mises} can be introduced to integrate the Von Mises criterion into the anisotropic failure criterion:

$$
\begin{aligned}
M &= \frac{6\sqrt{b^2-b+1}\sin\phi_{\text{mises}}}{3+(2b-1)\sin\phi_{\text{mises}}} = \frac{6\sin\phi}{3-\sin\phi} \\
\sin\phi_{\text{mises}} &= \frac{3\sin\phi}{3\sqrt{b^2-b+1}-\left(2b+\sqrt{b^2-b+1}-1\right)\sin\phi}
\end{aligned}
\tag{45}
$$

3.4.2. Tresca criterion

According to the Tresca criterion, the deviatoric stress at failure can be expressed as:

$$
q = \sqrt{3}\sin^{-1}\left(\theta+\frac{\pi}{3}\right)k = 2\sqrt{b^2-b+1}\cdot k \tag{46}
$$

where k is the maximum shear stress. Similar to the Von Mises criterion, a similar Tresca criterion can be integrated into the anisotropic failure criterion with the mobilized friction angle ϕ_{tresca}:

$$
M = \frac{6\sqrt{b^2-b+1}\sin\phi_{\text{tresca}}}{3+(2b-1)\sin\phi_{\text{tresca}}} = \frac{6\sqrt{b^2-b+1}\sin\phi}{3-\sin\phi}, \sin\phi_{\text{tresca}} = \frac{3\sin\phi}{3-2b\sin\phi} \tag{47}
$$

3.4.3. SMP criterion

The SMP failure criterion (Matsuoka and Nakai, 1974) can be integrated into the contact law to consider the effect of intermediate stress. According to Matsuoka and Nakai (1974), the SMP criterion can be expressed as:

$$
\frac{\tau_{\text{SMP}}}{\sigma_{\text{SMP}}} = \tan\phi_0 = \frac{2\sqrt{2}}{3}\tan\phi = \sqrt{\frac{I_1 I_2}{9I_3}-1} = \frac{2}{3}\sqrt{\tan^2\phi_{mo12}+\tan^2\phi_{mo13}+\tan^2\phi_{mo23}} \tag{48}
$$

where $\tan\phi_{moij} = \left(\sigma_i-\sigma_j\right)/\left(2\sqrt{\sigma_i\sigma_j}\right)$, I_1, I_2, and I_3 are the first, second, and third stress invariants. Defining $R=\sigma_1/\sigma_3$ denotes the ratio between major and minor principal stresses, $\tan\phi_{mo12}$ and $\tan\phi_{mo23}$ can be expressed as:

$$
\begin{aligned}
\tan\phi_{mo12} &= \frac{\sigma_1-\sigma_2}{2\sqrt{\sigma_1\sigma_2}} = \frac{\sigma_1-\sigma_3-b\left(\sigma_1-\sigma_3\right)}{2\sqrt{\sigma_1\sigma_3+b\sigma_1\left(\sigma_1-\sigma_3\right)}} = \frac{1-b}{\sqrt{1+bR-b}}\tan\phi_{mo13} \\
\tan\phi_{mo23} &= \frac{\sigma_2-\sigma_3}{2\sqrt{\sigma_2\sigma_3}} = \frac{b\left(\sigma_1-\sigma_3\right)}{2\sqrt{\sigma_3^2+b\sigma_3\left(\sigma_1-\sigma_3\right)}} = \frac{b\sqrt{R}}{\sqrt{1+bR-b}}\tan\phi_{mo13}
\end{aligned}
\tag{49}
$$

Substituting Eq. (49) into Eq. (48) leads to:

$$\frac{\tau_{\text{SMP}}}{\sigma_{\text{SMP}}} = \tan\phi_0 = \frac{2\sqrt{2}}{3}\tan\phi = \frac{2}{3}\sqrt{1+\frac{(1-b)^2+b^2R}{1+bR-b}}\tan\phi_{mo13} \tag{50}$$

Therefore, we can define a mobilized friction angle ϕ_{SMP} in the contact law to integrate the SMP criterion:

$$\tan\phi_{\text{SMP}} = \tan\phi_{mo13} = \sqrt{\frac{2}{1+\frac{(1-b)^2+b^2R}{1+bR-b}}}\tan\phi \tag{51}$$

3.4.4. Combination of different failure criteria

Similar to the weighted combination of the anisotropic strength proposed by Qin et al. (2024b), a weighted combination of the above friction angles can be used to integrate different failure criteria:

$$\sin\phi' = \omega_{\text{MC}}\sin\phi_{\text{MC}} + \omega_{\text{mises}}\sin\phi_{\text{mises}} + \omega_{\text{tresca}}\sin\phi_{\text{tresca}} + \omega_{\text{SMP}}\sin\phi_{\text{SMP}} \tag{52}$$

where ω_{MC}, ω_{mises}, ω_{tresca}, and ω_{SMP} are the weights for each criterion, ϕ_{MC} is the original Mohr–Coulomb friction angle ϕ. With the mobilized friction angle, the critical stress ratio can be expressed as:

$$M = \frac{6\sqrt{\tilde{b}^2-\tilde{b}+1}}{2-\tilde{b}}\,\frac{\left(2+\frac{1}{5}\tilde{F}_{11}\right)\sin\phi' - \left(1+\frac{2}{5}\tilde{F}_{22}\right)b'\sin\phi' + \frac{3}{5}\tilde{F}_{11}}{3+\left[2\left(1+\frac{2}{5}\tilde{F}_{22}\right)b' - \left(1-\frac{4}{5}\tilde{F}_{11}\right)\right]\sin\phi'} \tag{53}$$

From the analysis above, an anisotropic failure criterion, represented by Eq. (44), is proposed. The derivation is based solely on the relationship between stress and contact forces, as defined by the static hypothesis in Eq. (1) and the Love-Weber formula in Eq. (5). Fabric anisotropy is inherently accounted for within the Love-Weber formula without any additional consideration. The derivation demonstrates that the microscopic contact forces in each direction correspond to the macroscopic stress state in that direction. Under 2D conditions, the contact forces lie on a Mohr's circle, whereas under 3D conditions, they are contained within the region formed by three Mohr's circles. From this perspective, the micromechanical model describes the relationship between normal and shear forces on various inclined planes. Consequently, the micromechanical model reduces to the Mohr–Coulomb criterion for isotropic materials.

Although the failure criterion proposed in this paper is formulated based on the CH model, its analytical expression is independent of the CH model. This allows us to generalize any isotropic failure criterion to account for fabric anisotropy through the introduction of a mobilized friction angle which varies with the Lode angle, as shown in Eq. (53).

4. Parametric study

In this section, effects of degree of anisotropy and depositional direction on the anisotropic failure criterion shown in Eq. (53) will be discussed.

4.1. Effect of the degree of anisotropy

The deviatoric fabric tensor $\mathbf{F}$ for cross-anisotropic materials can be defined as:

$$\mathbf{F} = \begin{bmatrix} \Delta & 0 & 0 \\ 0 & -\frac{\Delta}{2} & 0 \\ 0 & 0 & -\frac{\Delta}{2} \end{bmatrix} \tag{54}$$

where Δ is a parameter representing the degree of anisotropy. Fig. 6 illustrates the influence of the degree of anisotropy on various failure criteria, assuming that the loading direction is coaxial with the material fabric.

It can be seen that the influence of fabric anisotropy is generally consistent for different failure criteria, although the shapes of the failure envelopes vary. For isotropic materials ($\Delta = 0$), the failure envelope is symmetric with respect to the three principal stresses. As Δ increases, the failure envelopes in sectors II and III shrink, whereas the failure envelope in sector I expands, indicating a reduction in shear strength within sectors II and III and an increase in shear strength within sector I. Furthermore, the combination of different failure criteria enhances the flexibility of the proposed failure criterion, thereby increasing the criterion's applicability.

4.2. Effect of the depositional direction

It is necessary to evaluate the failure criterion when the loading direction is not coaxial with the material fabric. Fig. 7 shows true triaxial conditions with inclined bedding plane.

Under this condition, the fabric tensor described in Eq. (54) must be rotated to align with the loading direction. Assuming the angle between the major principal stress and the major material axes is denoted by α, the fabric tensor should be rotated around the x_2-axis by an angle of α. This results in the following expression for the fabric tensor:

$$\mathbf{F}' = \mathbf{R}\mathbf{F}\mathbf{R}^{\top} \tag{55}$$

where $\mathbf{R}$ is the rotation matrix which is defined as:

$$\mathbf{R} = \begin{bmatrix} \cos\alpha & 0 & \sin\alpha \\ 0 & 1 & 0 \\ -\sin\alpha & 0 & \cos\alpha \end{bmatrix} \tag{56}$$

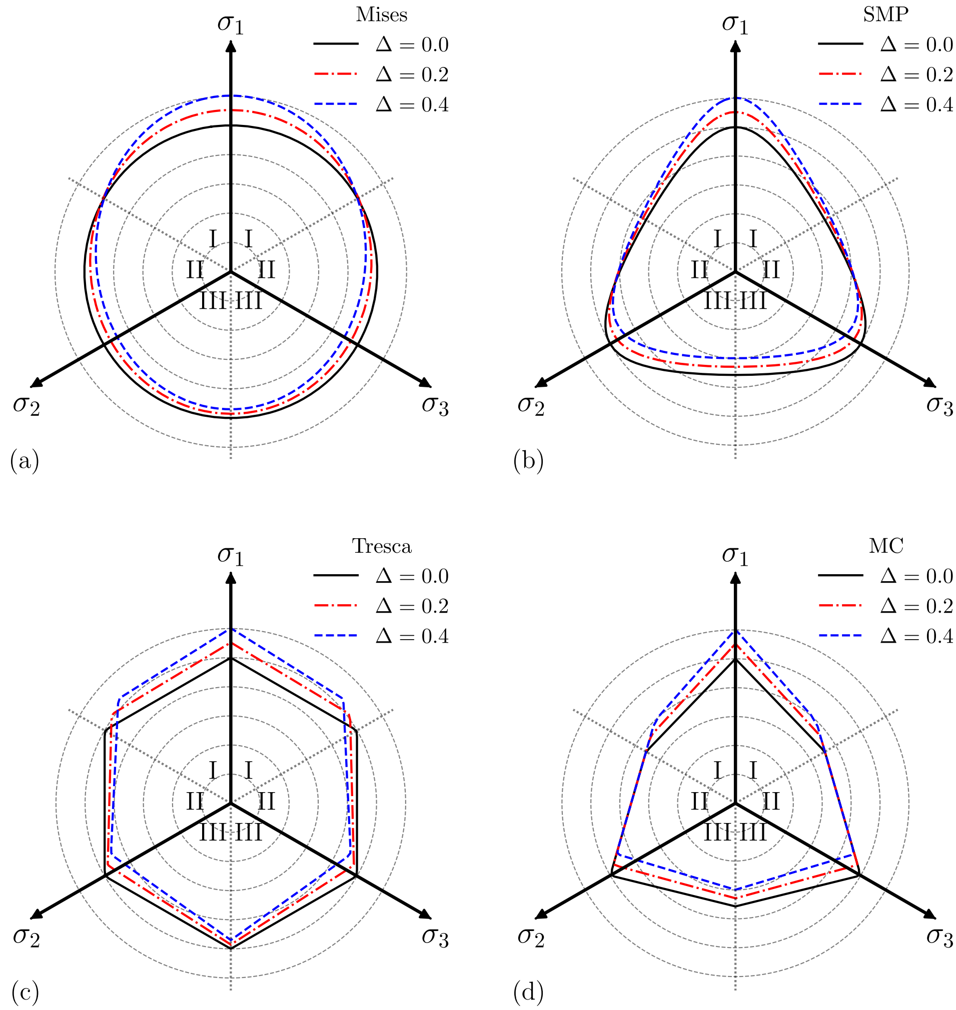

Fig. 6. Effect of anisotropy degree for different failure criteria: (a) Von Mises criterion; (b) SMP criterion; (c) Tresca criterion; (d) Mohr–Coulomb criterion.

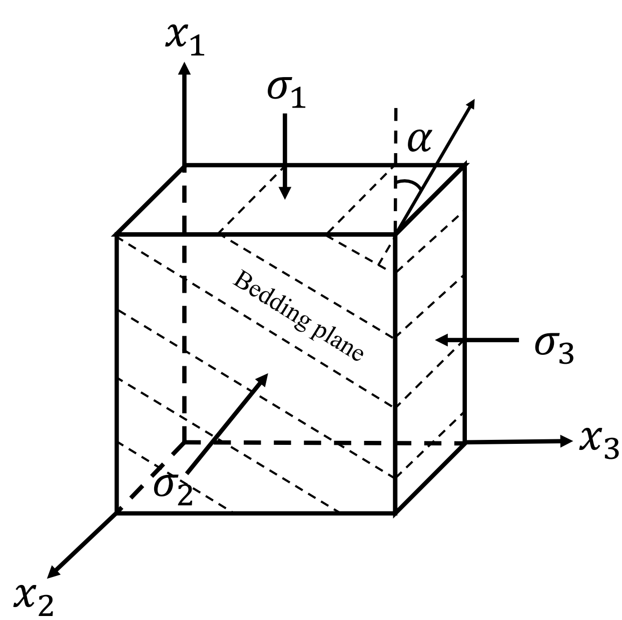

Fig. 7. True triaxial conditions with inclined bedding plane.

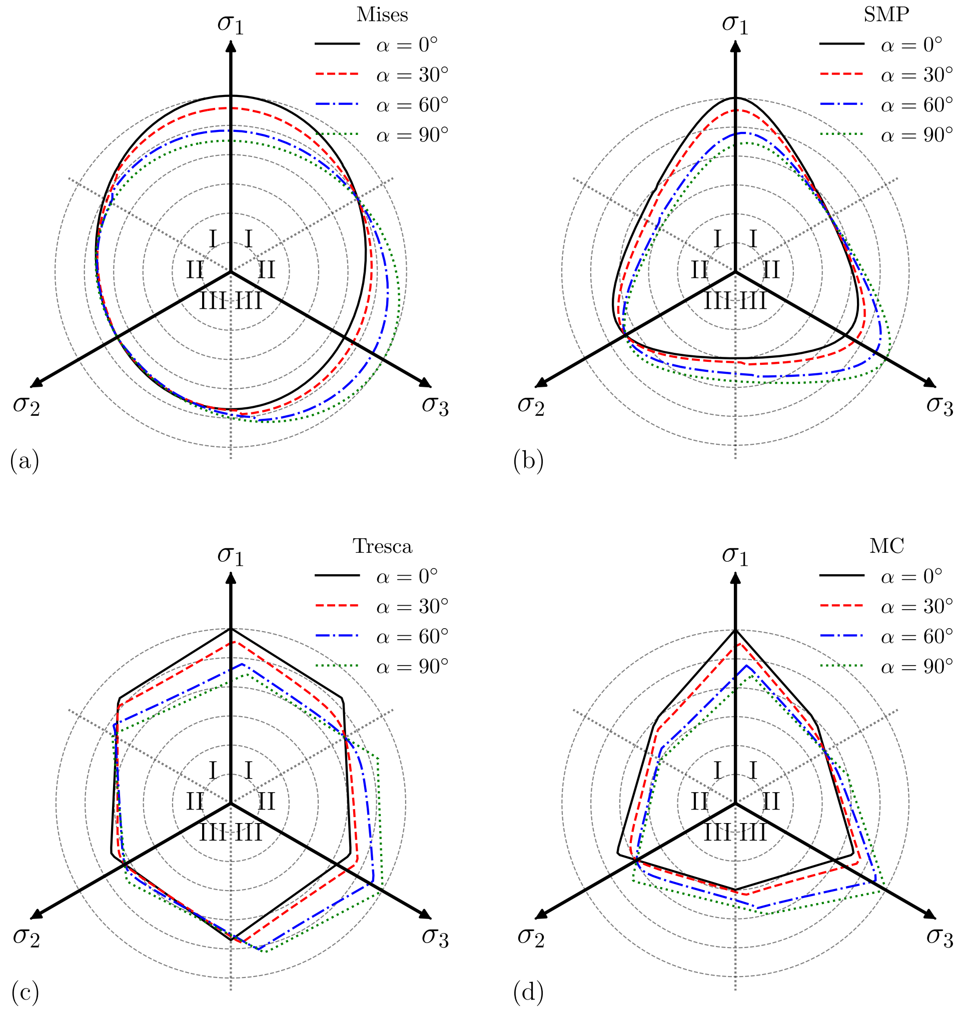

Fig. 8. Effect of depositional direction for different failure criteria: (a) Von Mises criterion; (b) SMP criterion; (c) Tresca criterion; (d) Mohr–Coulomb criterion.

Then, the rotated fabric tensor $\mathbf{F}'$ can be used in the proposed failure criterion. Fig. 8 shows the effect of depositional direction for different failure criteria with $\Delta = 0.4$.

It can be observed that the influence of depositional direction appears to be generally consistent for various failure criteria, although the shapes of the failure envelopes differ. When $\alpha = 90°$, the major material axis shifts to σ_3 axis, and the failure envelope becomes symmetric about the σ_2 axis, resembling the failure envelope observed when $\alpha = 0°$. Similarly, the failure envelopes for inclined angles of 30° and 60° are symmetric about the σ_2 axis. Interestingly, the failure envelopes of the Tresca and Mohr–Coulomb criteria exhibit curvature when the inclined angles are not equal to 0° or 90°, which can be attributed to the effect of the intermediate principal stress on the major and minor principal stresses in the modified stress space. This observation aligns with the findings of Tian and Yao (2017).

5. Validation of the failure criterion

The SMP criterion is widely employed to simulate failure envelopes for both isotropic and anisotropic materials (Xiao et al., 2012; Kong et al., 2013; Chen et al., 2020; Wang et al., 2020). Additionally, the Von Mises criterion is often integrated with the SMP criterion (Yao et al., 2004; Gao et al., 2010; Tian and Yao, 2017) to improve its applicability. Therefore, the SMP and Von Mises criteria are used together in this study. Four sets of true triaxial test data (Ochiai and Lade, 1983; Kirkgard and Lade, 1993; Abelev and Lade, 2004; Haruyama, 1981) are utilized for the simulation. Table 3 presents the calibrated parameters of the proposed failure criterion, which integrates the Von Mises and SMP criteria while assuming a cross-anisotropic fabric. Due to gravitational deposition processes, soils typically exhibit cross-anisotropic fabric. Under true triaxial conditions, the soil fabric may evolve toward orthotropy according to the anisotropic critical state theory (ACST) framework (Li and Dafalias, 2012). Therefore, the following orthotropic fabric tensor is used in the following simulations:

$$\mathbf{F} = \begin{bmatrix} F_{11} & 0 & 0 \\ 0 & F_{22} & 0 \\ 0 & 0 & F_{33} \end{bmatrix} \tag{57}$$

Table 3 presents calibrated model parameters for the proposed failure criterion.

Table 3
Summary of calibrated model parameters for true triaxial tests.

Soil	Reference	ϕ (°)	F_{11}	F_{22}	F_{33}	ω_{mises}	ω_{SMP}
Cambria sand	Ochiai and Lade (1983)	39.76	0.108	0.020	−0.128	0.259	0.741
San Francisco Bay mud	Kirkgard and Lade (1993)	38.64	0.339	−0.096	−0.243	0.117	0.883
Santa Monica Beach sand	Abelev and Lade (2004)	45.60	0.324	−0.060	−0.264	0.161	0.839
Glass beads	Haruyama (1981)	28.68	0.285	−0.112	−0.173	0.445	0.555

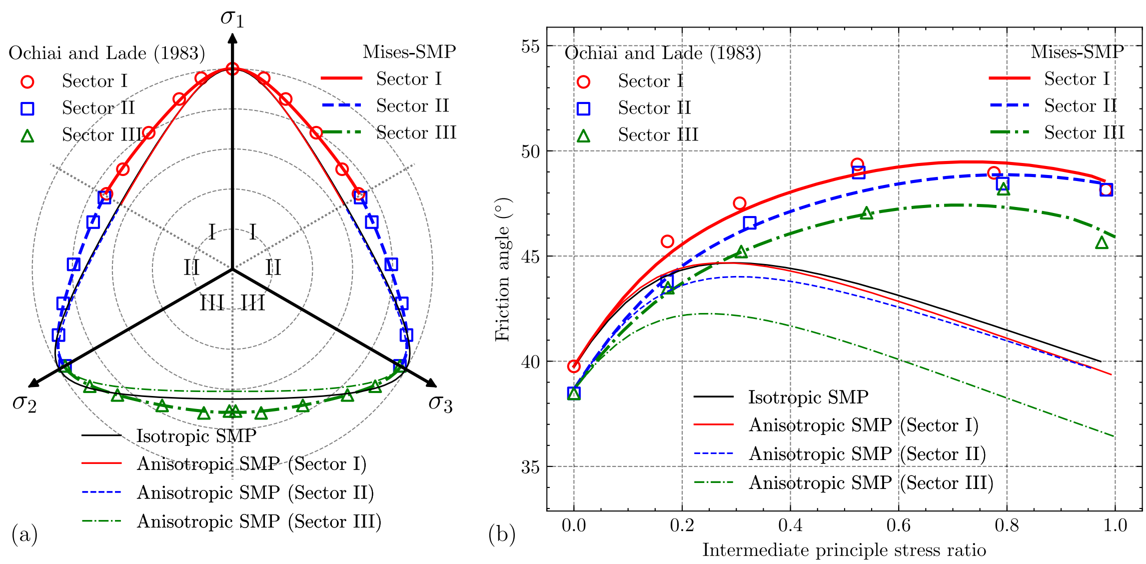

Fig. 9. Comparison between predictions and experiments by Ochiai and Lade (1983): (a) π plane; (b) friction angle.

5.1. Cambria sand

Ochiai and Lade (1983) conducted true triaxial tests with the back pressure of 100 kPa on uniformly graded Cambria sand with particle sizes ranging from 0.84 mm to 2.00 mm, a specific gravity of 2.708, and minimum and maximum void ratios of 0.51 and 0.80. The comparison between experiments by Ochiai and Lade (1983) and predictions by the failure criterion, along with the isotropic and anisotropic SMP criterion, is showed in Fig. 9. The results indicate that the effect of fabric anisotropy on the failure envelope is minimal, as the failure envelopes in the three sectors are closely aligned. Within each sector, the friction angle is smallest under conventional triaxial compression conditions ($b = 0$). The friction angle increases with b until it reaches approximately 0.7, after which a slight decrease is observed as b approaches 1. A comparison of experimental results and predictions demonstrates that the proposed failure criterion accurately predicts friction angles for all three sectors, except for a slight overestimation in Sector III when b approaches 1. These findings are consistent with those reported by Gao et al. (2010), who applied a generalized anisotropic strength criterion. This similarity arises because the generalized anisotropic strength criterion is derived from the generalized nonlinear strength theory (GNST; Yao et al. (2004)) by incorporating a fabric anisotropy variable. GNST is based on the Von Mises and SMP criteria, both of which are also employed in this paper. The key difference lies in the method of combining these criteria: GNST averages the deviatoric stresses, whereas this study averages the friction angles.

5.2. San Francisco Bay mud

Although the CH micromechanical model was primarily developed for sand, the derived anisotropic failure criterion can be applied for clay and mud because it does not depend on the CH micromechanical framework. Kirkgard and Lade (1993) conducted true triaxial tests on San Francisco Bay mud with a back pressure of 200 kPa, a unit weight of 1.44 g/cm^3, and a water content of 98.5%. The comparison between experiments by Kirkgard and Lade (1993) and predictions by the failure criterion, along with the isotropic and anisotropic SMP criterion, is showed in Fig. 10. The results reveal that fabric anisotropy had a significant effect compared to Cambria sand, as the friction angle in sectors II and III are notably smaller than that in sector I. The experimental results show good agreement with predictions, except for a slight underestimation of the friction angle in sector II when the b value ranges from 0.2 to 0.7. This finding differs from those of Gao et al. (2010), who predicted an overestimation of the friction angle in sector III. While the friction angle differences are negligible for conventional triaxial compression and extension tests, the friction angles obtained under true triaxial conditions are slightly higher than those from conventional tests. These results are closely aligned with the SMP criterion, as confirmed by the predictions of the anisotropic SMP criterion illustrated in Fig. 10. Similarly, Kong et al. (2013) demonstrated that the anisotropic SMP criterion could accurately simulate the true triaxial test results reported by Kirkgard and Lade (1993).

5.3. Santa Monica Beach sand

Abelev and Lade (2004) conducted true triaxial tests on San Francisco Bay mud with a back pressure of 50 kPa and a void ratio of 0.6 ($D_r = 90\%$). The comparison between experiments by Abelev and Lade (2004) and predictions by the failure criterion, along with the isotropic and anisotropic SMP criterion, is showed in Fig. 11. The results indicate that the proposed failure criterion aligns well with experimental data, except for a slight

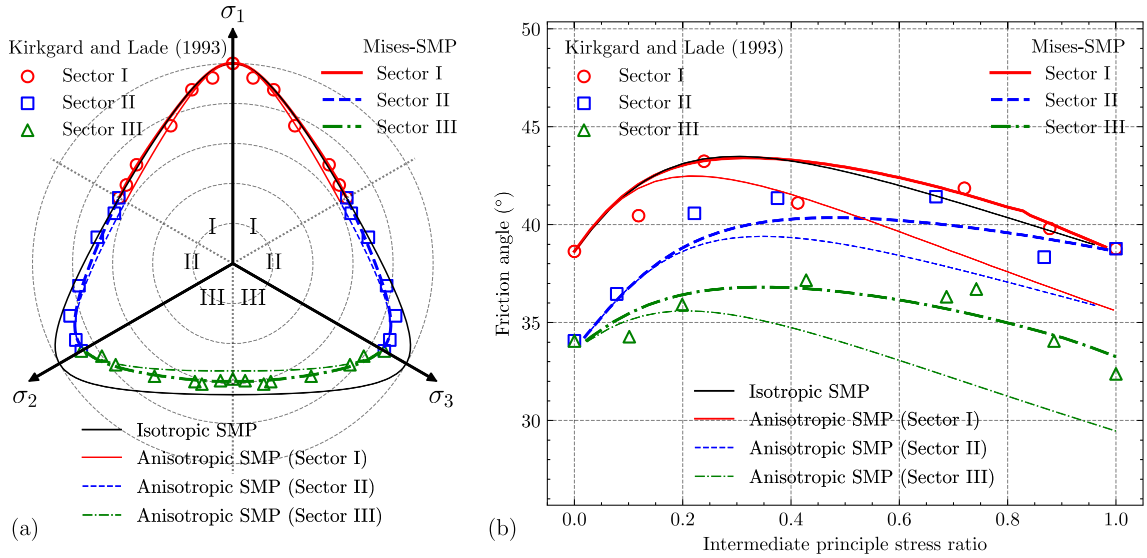

Fig. 10. Comparison between predictions and experiments by Kirkgard and Lade (1993): (a) π plane; (b) friction angle.

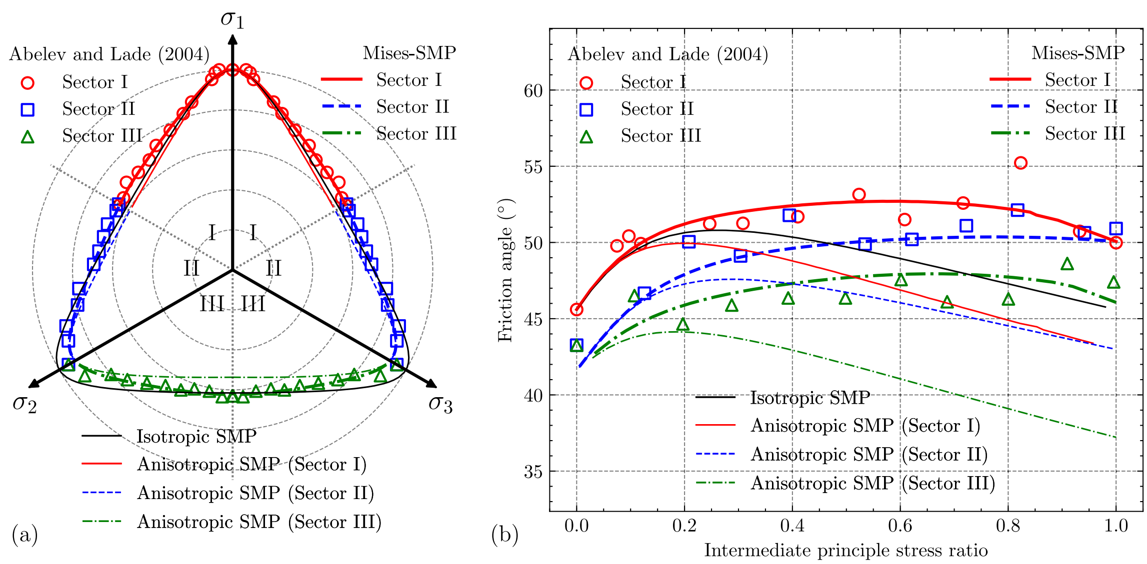

Fig. 11. Comparison between predictions and experiments by Abelev and Lade (2004): (a) π plane; (b) friction angle.

overestimation of the friction angle in sector II when the b value ranges from 0.2 to 0.7. This behavior is consistent with experiments on San Francisco Bay mud discussed above. The influence of fabric anisotropy is significant, similar observations are found for experiments on San Francisco Bay mud as discussed before. Furthermore, the friction angle varies between triaxial compression and extension conditions, with the friction angle under triaxial extension conditions being slightly larger than that under triaxial compression. Notably, according to Lade (2007) and Gao et al. (2010), the friction angle is overestimated in the middle range of b values for all three sectors. They attribute this to the formation of shear bands, which reduce shear strength and consequently lower the friction angle. Overall, the proposed failure criterion demonstrates a superior ability to simulate general failure modes compared to the criteria proposed by Lade (2007) and Gao et al. (2010). While the generalized anisotropic strength criterion by Gao et al. (2010) combines the Von Mises and SMP criteria, similar to the failure criterion in this study, the latter offers improved predictive performance.

5.4. Glass beads

Haruyama (1981) conducted true triaxial tests on glass beads under a mean stress of 98 kPa, with particle sizes ranging from 0.125 mm to 0.42 mm, a specific gravity of 2.476, and a void ratio of 0.719 (D_r = 95%, $e_{\min}$ = 0.491, $e_{\max}$ = 0.731). The comparison between experiments by Haruyama (1981) and predictions by the failure criterion, along with the isotropic and anisotropic SMP criterion, is showed in Fig. 12. The results demonstrate that the proposed failure criterion aligns well with the experimental data. The influence of fabric anisotropy is significant, consistent with findings from experiments on San Francisco Bay mud and Santa Monica Beach sand. Chen et al. (2020) introduced an anisotropic SMP criterion based on the TS method and applied it to simulate experiments on glass beads. According to Chen et al. (2020), the anisotropic SMP criterion underestimates the friction angle in sector I and overestimates it in sectors II and III. In contrast, the proposed criterion, which

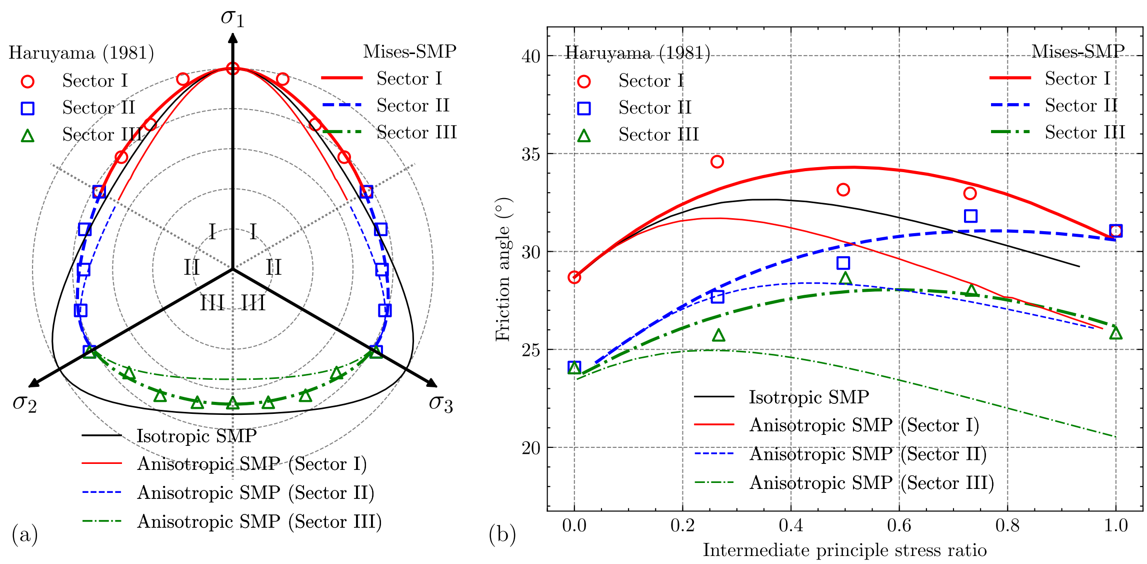

Fig. 12. Comparison between predictions and experiments by Haruyama (1981): (a) π plane; (b) friction angle.

Table 4
Model parameters for hollow cylinder torsional tests on Toyoura sand.

k_{n0} (N/mm)	n_e	k_{rR}	k_{pR}	ϕ_c (°)	e_{ref}	λ	ξ	n_p	n_d	A_d	Δ	c	r
80	0.71	0.31	0.32	27.6	0.934	0.019	0.7	1.15	0.58	0.51	0.43	3.63	1

combines the Von Mises and SMP criteria, provides more accurate predictions of the friction angle. This demonstrates that incorporating the Von Mises criterion is essential for accurately predicting general failure modes while accounting for fabric anisotropy.

5.5. Discussions

To summarize, the discussions above demonstrate that the proposed failure criterion effectively simulates true triaxial tests for various soils. The influence of fabric anisotropy differs for different soils. For San Francisco Bay mud, Santa Monica Beach sand, and glass beads, significant anisotropic effects are observed, as the friction angles in sector II and sector II are noticeably smaller than those in Sector I. In contrast, Cambria sand exhibits minimal fabric anisotropy effects. Additionally, the parameter ω_{mises} as shown in Table 3 highlights the necessity of incorporating the Von Mises criterion for Cambria sand and glass beads. Experimental data further indicate that the stress ratio between triaxial extension and triaxial compression exceeds the corresponding stress ratio predicted by the SMP (or Mohr–Coulomb) criterion.

6. Extension of the failure criterion

The above analysis focuses on the shape of the failure envelope in π plane. Combined with a contact law shown in Table 1 and an evolution law for the fabric tensor, the CH micromechanical model can effectively capture the complex behaviors of granular materials under various loading conditions. For simplicity, the following fabric evolution law is adopted in this paper (Li and Dafalias, 2012):

$$\mathrm{d}\mathbf{F} = \langle \lambda \rangle (\mathbf{n} - r\mathbf{F}) \tag{58}$$

where c and r are the fabric evolution parameters, $\langle \lambda \rangle$ is the norm of deviatoric plastic strain increment $\|\mathrm{d}\varepsilon_q^p\|$ and $\mathbf{n}$ is the loading direction which is usually taken as the direction of deviatoric plastic flow. More specifically, the loading direction $\mathbf{n}$ is defined as $\mathrm{d}\varepsilon_q^p/\|\mathrm{d}\varepsilon_q^p\|$ in this paper. At critical state, the fabric tensor $\mathbf{F}$ is coaxial with the loading direction $\mathbf{n}$ and the fabric anisotropy variable A approaches 1 (Li and Dafalias, 2012):

$$A = \mathbf{F} : \mathbf{n} = F\mathbf{n}_F : \mathbf{n} = FN \tag{59}$$

where $\mathbf{n}_F$ is the direction of the fabric tensor, F is the norm of the fabric tensor and N is the norm of the loading direction.

Hollow cylinder torsional tests (Yoshimine et al., 1998) were employed to assess the model's performance. The experiments were conducted on Toyoura sand (d_{50} = 0.17 mm, e_0 = 0.861 − 0.890) under a confining pressure of 100 kPa. As Li and Dafalias (2012) demonstrated, hollow cylinder torsional tests can be simulated using undrained triaxial compression and extension tests, in which the principal stress directions oriented at varying angles (α) relative to the initial principal axes of the fabric tensor. The model parameters for the tests are summarized in Table 4.

Figs. 13 and 14 present simulation results for undrained triaxial compression and extension tests on Toyoura sand under varying loading directions. The figures demonstrate that the model accurately captures the influence of loading direction on the mechanical behavior of Toyoura sand with the fabric evolution law. As the angle α increases, the soil softens and its strength decreases. Moreover, when α exceeds 45°, the soil tend to exhibit static liquefaction. However, subsequent fabric changes cause the stress–strain curve to turn-back and the soil to regain strength.

Fig. 15 shows the evolution of the fabric anisotropy variable A and the norm of the fabric tensor F. As axial strain increases, both A and F approach 1, indicating that Toyoura sand reaches the anisotropic critical state at large strains. When α = 90°, the norm of the fabric tensor F initially decreases to 0 before gradually increasing to 1. For α values between 60° and 90°, F first decreases to a minimum value before gradually increasing to 1. This shows that the larger α is, the easier it is for the soil to tend to be isotropic initially, and then gradually approach to the anisotropic critical state. The increasing fabric anisotropy finally increases the soil's strength as shown in Fig. 14.

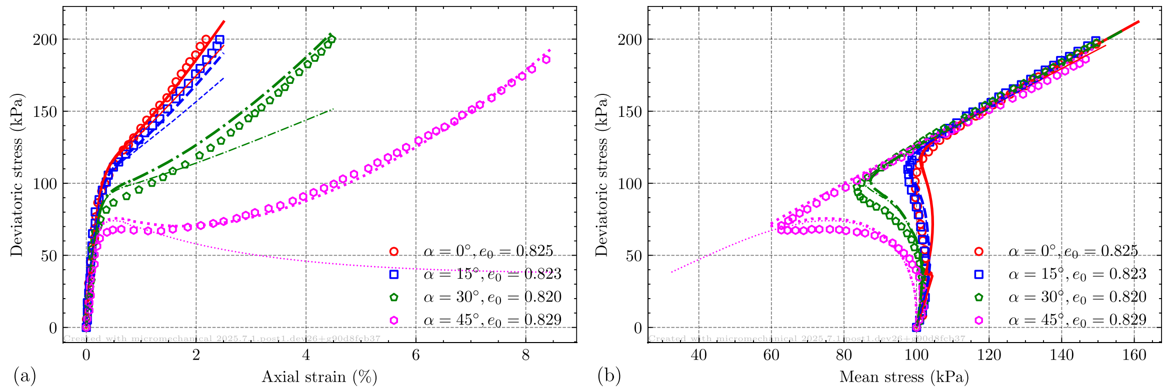

Fig. 13. Comparison between simulations and experiments for the undrained triaxial compression tests on Toyoura sand (thicker lines represent simulations with fabric evolution, thinner lines represent simulations without fabric evolution): (a) axial strain vs. deviatoric stress; (b) mean stress vs. deviatoric stress.

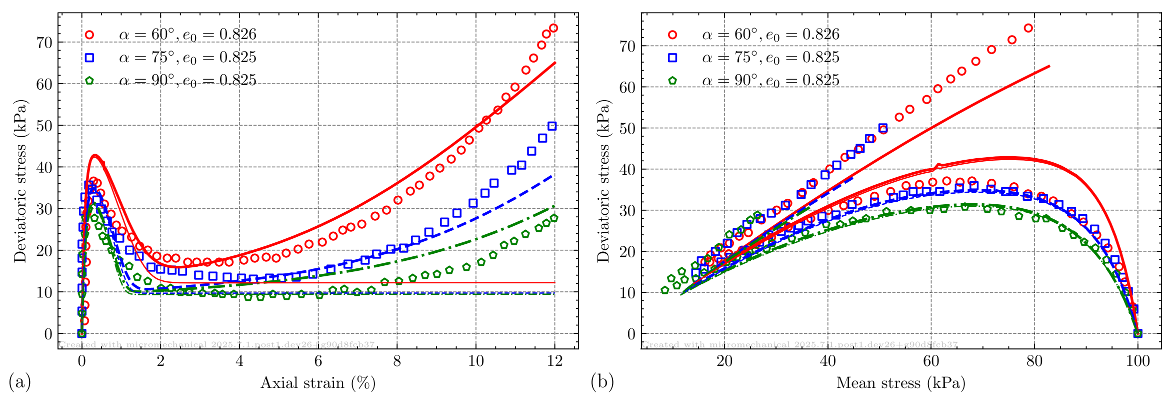

Fig. 14. Comparison between simulations and experiments for the undrained triaxial extension tests on Toyoura sand (thicker lines represent simulations with fabric evolution, thinner lines represent simulations without fabric evolution): (a) axial strain vs. deviatoric stress; (b) mean stress vs. deviatoric stress.

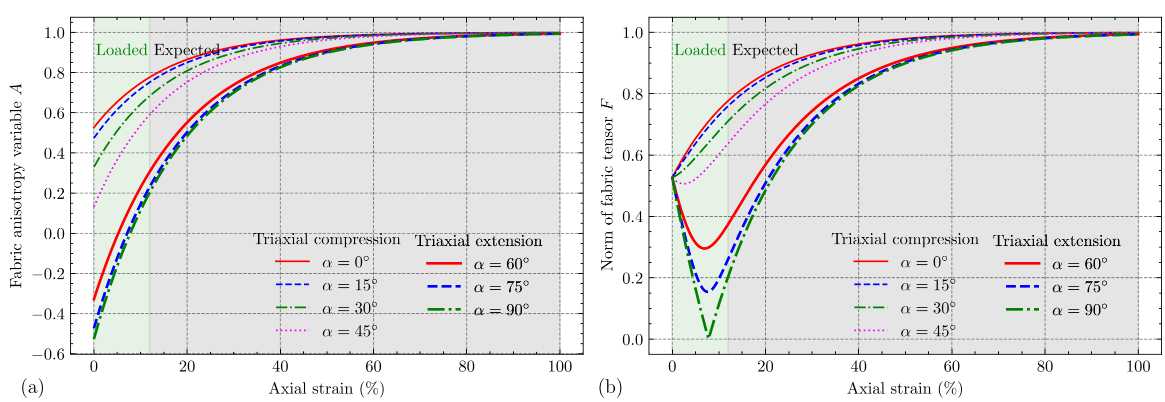

Fig. 15. Evolution of fabric anisotropy for Toyoura sand: (a) fabric anisotropy variable; (b) norm of fabric anisotropy.

7. Conclusions

In this paper, an anisotropic failure criterion is proposed based on the CH micromechanical model. The main contributions of the study are as follows:

- A new anisotropic failure criterion is derived from the CH micromechanical model. The derivation relies solely on the relationship between stress and contact forces, as described by the static hypothesis and the Love-Weber equation. For isotropic materials, the proposed failure criterion is shown to be identical to the classical Mohr–Coulomb criterion.
- The fabric anisotropy is inherently incorporated into the failure criterion through the Love-Weber equation with the introduction of the fabric tensor.
- To enhance the applicability of the failure criterion, the Von Mises, Tresca, and SMP criteria are integrated into the new failure criterion using a mobilized friction angle, resulting in a flexible representation of failure envelopes.

- True triaxial tests from the literature are used to evaluate the proposed failure criterion. The results demonstrate that the failure criterion effectively predicts failure envelopes under true triaxial conditions.
- A fabric evolution law is proposed in the CH micromechanical model and hollow cylinder torsional tests on Toyoura sand are simulated. The results show that the model accurately captures the influence of loading direction on the mechanical behavior of granular materials.

CRediT authorship contribution statement

Hai-Lin Wang: Writing – review & editing, Writing – original draft, Visualization, Methodology, Investigation, Formal analysis, Conceptualization. **Xiaoqiang Gu:** Writing – review & editing, Supervision, Funding acquisition, Conceptualization. **Zhen-Yu Yin:** Writing – review & editing, Supervision, Conceptualization.

Declaration of Generative AI and AI-assisted technologies in the writing process

During the preparation of this work, the authors used DeepSeek in order to improve readability and language of the paper. After using this tool, the authors reviewed and edited the content as needed and take full responsibility for the content of the publication.

Declaration of competing interest

The authors declare that they have no known competing financial interests or personal relationships that could have appeared to influence the work reported in this paper.

Acknowledgments

The work presented in this paper is supported by National Natural Science Foundation of China (Grant No. 51822809 and 42361164615), the Fundamental Research Funds for the Central Universities, China and the Research Grants Council (RGC) of Hong Kong (Grant No. 15217220 and N_PolyU534/20). These supports are gratefully acknowledged.

Data availability

Data will be made available on request.

References

Abelev, A.V., Lade, P.V., 2004. Characterization of failure in cross-anisotropic soils. J. Eng. Mech. 130 (5), 599–606. http://dx.doi.org/10.1061/(ASCE)0733-9399(2004)130:5(599).

Bignonnet, F., Dormieux, L., Kondo, D., 2016. A micro-mechanical model for the plasticity of porous granular media and link with the Cam clay model. Int. J. Plast. 79, 259–274. http://dx.doi.org/10.1016/j.ijplas.2015.07.003.

Chang, C.S., Hicher, P.Y., 2005. An elasto-plastic model for granular materials with microstructural consideration. Int. J. Solids Struct. 42 (14), 4258–4277. http://dx.doi.org/10.1016/j.ijsolstr.2004.09.021.

Chang, C.S., Hicher, P.Y., Yin, Z.Y., Kong, L.R., 2009. Elastoplastic model for clay with microstructural consideration. J. Eng. Mech. 135 (9), 917–931. http://dx.doi.org/10.1061/(ASCE)EM.1943-7889.0000013.

Chang, C.S., Yin, Z.-Y., 2010. Micromechanical modeling for inherent anisotropy in granular materials. J. Eng. Mech. 136 (7), 830–839. http://dx.doi.org/10.1061/(ASCE)EM.1943-7889.0000125.

Chen, H., Wang, Y., Li, J., Sun, D., 2020. A general failure criterion for soil considering three-dimensional anisotropy. Comput. Geotech. 125, 103691. http://dx.doi.org/10.1016/j.compgeo.2020.103691.

Dafalias, Y.F., Manzari, M.T., 2004. Simple plasticity sand model accounting for fabric change effects. J. Eng. Mech. 130 (6), 622–634. http://dx.doi.org/10.1061/(ASCE)0733-9399(2004)130:6(622).

Dafalias, Y.F., Manzari, M.T., Papadimitriou, A.G., 2006. SANICLAY: Simple anisotropic clay plasticity model. Int. J. Numer. Anal. Methods Geomech. 30 (12), 1231–1257. http://dx.doi.org/10.1002/nag.524.

Dafalias, Y.F., Papadimitriou, A.G., Li, X.S., 2004. Sand plasticity model accounting for inherent fabric anisotropy. J. Eng. Mech. 130 (11), 1319–1333. http://dx.doi.org/10.1061/(ASCE)0733-9399(2004)130:11(1319).

Desmorat, R., Marull, R., 2011. Non-quadratic Kelvin modes based plasticity criteria for anisotropic materials. Int. J. Plast. 27 (3), 328–351. http://dx.doi.org/10.1016/j.ijplas.2010.06.003.

Dong, T., Kong, L., Zhe, M., Zheng, Y., 2019. Anisotropic failure criterion for soils based on equivalent stress tensor. Soils Found. 59 (3), 644–656. http://dx.doi.org/10.1016/j.sandf.2019.02.001.

Ganesan, G., Mishra, A.K., 2024. A modified anisotropic Hoek and Brown failure criterion for transversely isotropic rocks. Geotech. Geol. Eng. 42 (6), 4869–4889. http://dx.doi.org/10.1007/s10706-024-02818-0.

Gao, Z., Ma, P., Tang, Y., Chen, Y., Ma, Q., 2024. A novel constitutive model of the anisotropic sand accounting for the fabric evolution. Comput. Geotech. 176, 106797. http://dx.doi.org/10.1016/j.compgeo.2024.106797.

Gao, Z., Zhao, J., 2017. A non-coaxial critical-state model for sand accounting for fabric anisotropy and fabric evolution. Int. J. Solids Struct. 106–107, 200–212. http://dx.doi.org/10.1016/j.ijsolstr.2016.11.019.

Gao, Z., Zhao, J., Li, X.-S., Dafalias, Y.F., 2014. A critical state sand plasticity model accounting for fabric evolution. Int. J. Numer. Anal. Methods Geomech. 38 (4), 370–390. http://dx.doi.org/10.1002/nag.2211.

Gao, Z., Zhao, J., Yao, Y., 2010. A generalized anisotropic failure criterion for geomaterials. Int. J. Solids Struct. 47 (22), 3166–3185. http://dx.doi.org/10.1016/j.ijsolstr.2010.07.016.

Görthofer, J., Schneider, M., Hrymak, A., Böhlke, T., 2022. A computational multiscale model for anisotropic failure of sheet molding compound composites. Compos. Struct. 288, 115322. http://dx.doi.org/10.1016/j.compstruct.2022.115322.

Haruyama, M., 1981. Anisotropic deformation-strength characteristics of an assembly of spherical particles under three dimensional stresses. Soils Found. 21 (4), 41–55. http://dx.doi.org/10.3208/sandf1972.21.4_41.

Hicher, P.Y., Chang, C.S., 2007. A microstructural elastoplastic model for unsaturated granular materials. Int. J. Solids Struct. 44 (7), 2304–2323. http://dx.doi.org/10.1016/j.ijsolstr.2006.07.007.

Hoek, E., Brown, E.T., 1980. Empirical strength criterion for rock masses. J. Geotech. Eng. Div. 106 (9), 1013–1035. http://dx.doi.org/10.1061/AJGEB6.0001029.

Huang, S., Zhang, J., Ding, X., Zhang, C., Han, G., Yu, G., Qu, L., 2024. Investigation of anisotropic strength criteria for layered rock mass. J. Rock Mech. Geotech. Eng. 16 (4), 1289–1304. http://dx.doi.org/10.1016/j.jrmge.2023.06.006.

Ismael, M., Konietzky, H., 2019. Constitutive model for inherent anisotropic rocks: Ubiquitous joint model based on the Hoek-Brown failure criterion. Comput. Geotech. 105, 99–109. http://dx.doi.org/10.1016/j.compgeo.2018.09.016.

Iyanaga, S., Kawada, Y., 1993. Encyclopedic Dictionary of Mathematics, vol. 1, MIT Press.

Karafillis, A.P., Boyce, M.C., 1993. A general anisotropic yield criterion using bounds and a transformation weighting tensor. J. Mech. Phys. Solids 41 (12), 1859–1886. http://dx.doi.org/10.1016/0022-5096(93)90073-O.

Kirkgard, M., Lade, P., 1993. Anisotropic three-dimensional behavior of a normally consolidated clay. Can. Geotech. J. 30 (5), 848–858. http://dx.doi.org/10.1139/t93-075.

Kong, Y., Zhao, J., Yao, Y., 2013. A failure criterion for cross-anisotropic soils considering microstructure. Acta Geotech. 8 (6), 665–673. http://dx.doi.org/10.1007/s11440-012-0202-7.

Lade, P.V., 2007. Modeling failure in cross-anisotropic frictional materials. Int. J. Solids Struct. 44 (16), 5146–5162. http://dx.doi.org/10.1016/j.ijsolstr.2006.12.027.

Lade, P.V., Duncan, J.M., 1975. Elastoplastic stress-strain theory for cohesionless soil. J. Geotech. Eng. Div. 101 (10), 1037–1053. http://dx.doi.org/10.1061/AJGEB6.0000204.

Lam, W.-K., Tatsuoka, F., 1988. Effects of initial anisotropic fabric and $\sigma 2$ on strength and deformation characteristics of sand. Soils Found. 28 (1), 89–106. http://dx.doi.org/10.3208/sandf1972.28.89.

Leoni, M., Karstunen, M., Vermeer, P.A., 2008. Anisotropic creep model for soft soils. Géotechnique 58 (3), 215–226. http://dx.doi.org/10.1680/geot.2008.58.3.215.

Li, X.S., Dafalias, Y.F., 2002. Constitutive modeling of inherently anisotropic sand behavior. J. Geotech. Geoenvironmental Eng. 128 (10), 868–880. http://dx.doi.org/10.1061/(ASCE)1090-0241(2002)128:10(868).

Li, X.S., Dafalias, Y.F., 2012. Anisotropic critical state theory: Role of fabric. J. Eng. Mech. 138 (3), 263–275. http://dx.doi.org/10.1061/(ASCE)EM.1943-7889.0000324.

Li, H., Pel, L., You, Z., Smeulders, D., 2024. Stress-dependent instantaneous cohesion and friction angle for the Mohr–Coulomb criterion. Int. J. Mech. Sci. 283, 109652. http://dx.doi.org/10.1016/j.ijmecsci.2024.109652.

Liao, D., Yang, Z., 2021a. Non-coaxial hypoplastic model for sand with evolving fabric anisotropy including non-proportional loading. Int. J. Numer. Anal. Methods Geomech. 45 (16), 2433–2463. http://dx.doi.org/10.1002/nag.3272.

Liao, D., Yang, Z.X., 2021b. Hypoplastic modeling of anisotropic sand behavior accounting for fabric evolution under monotonic and cyclic loading. Acta Geotech. 16 (7), 2003–2029. http://dx.doi.org/10.1007/s11440-020-01127-z.

Liu, H., Han, Z., Han, Z., Chen, Z., Liu, Q., Zhang, H., Zhang, R., Guo, L., 2024. Nonlinear empirical failure criterion for rocks under triaxial compression. Int. J. Min. Sci. Technol. 34 (3), 351–369. http://dx.doi.org/10.1016/j.ijmst.2024.03.002.

Lou, Y., Yoon, J.W., 2017. Anisotropic ductile fracture criterion based on linear transformation. Int. J. Plast. 93, 3–25. http://dx.doi.org/10.1016/j.ijplas.2017.04.008.

Lou, Y., Yoon, J.W., 2021. A user-friendly anisotropic ductile fracture criterion for sheet metal under proportional loading. Int. J. Solids Struct. 217–218, 48–59. http://dx.doi.org/10.1016/j.ijsolstr.2021.01.017.

Love, A.E.H., 1927. A Treatise on the Mathematical Theory of Elasticity. University Press.

Matsuoka, H., Nakai, T., 1974. Stress-deformation and strength characteristics of soil under three different principal stresses. Proc. Jpn. Soc. Civ. Eng. 1974 (232), 59–70. http://dx.doi.org/10.2208/jscej1969.1974.232_59.

Mortara, G., 2008. A new yield and failure criterion for geomaterials. Géotechnique 58 (2), 125–132. http://dx.doi.org/10.1680/geot.2008.58.2.125.

Mortara, G., 2010. A yield criterion for isotropic and cross-anisotropic cohesive-frictional materials. Int. J. Numer. Anal. Methods Geomech. 34 (9), 953–977. http://dx.doi.org/10.1002/nag.846.

Nguyen, P.H., Le, C.V., 2021. Failure analysis of anisotropic materials using computational homogenised limit analysis. Comput. Struct. 256, 106646. http://dx.doi.org/10.1016/j.compstruc.2021.106646.

Ochiai, H., Lade, P.V., 1983. Three-dimensional behavior of sand with anisotropic fabric. J. Geotech. Eng. 109 (10), 1313–1328. http://dx.doi.org/10.1061/(ASCE)0733-9410(1983)109:10(1313).

Papadimitriou, A.G., Chaloulos, Y.K., Dafalias, Y.F., 2019. A fabric-based sand plasticity model with reversal surfaces within anisotropic critical state theory. Acta Geotech. 14 (2), 253–277. http://dx.doi.org/10.1007/s11440-018-0751-5.

Pei, J., Einstein, H.H., Whittle, A.J., 2018. The normal stress space and its application to constructing a new failure criterion for cross-anisotropic geomaterials. Int. J. Rock Mech. Min. Sci. 106, 364–373. http://dx.doi.org/10.1016/j.ijrmms.2018.03.023.

Petalas, A.L., Dafalias, Y.F., Papadimitriou, A.G., 2019. SANISAND-FN: An evolving fabric-based sand model accounting for stress principal axes rotation. Int. J. Numer. Anal. Methods Geomech. 43 (1), 97–123. http://dx.doi.org/10.1002/nag.2855.

Pietruszczak, S., Mroz, Z., 2000. Formulation of anisotropic failure criteria incorporating a microstructure tensor. Comput. Geotech. 26 (2), 105–112. http://dx.doi.org/10.1016/S0266-352X(99)00034-8.

Qin, Q., Li, K., Li, M., Abbas, N., Yue, R., Qiu, S., 2024a. An anisotropic failure criterion for jointed rocks under triaxial stress conditions. Rock Mech. Rock Eng. 57 (5), 3121–3138. http://dx.doi.org/10.1007/s00603-023-03684-7.

Qin, Q., Li, K., Li, M., Wu, S., Abbas, N., Yue, R., 2024b. A weight combination anisotropic strength criterion considering the effect of joint orientation. Acta Geotech. http://dx.doi.org/10.1007/s11440-024-02467-w.

Schweiger, H.F., Wiltafsky, C., Scharinger, F., Galavi, V., 2009. A multilaminate framework for modelling induced and inherent anisotropy of soils. Géotechnique 59 (2), 87–101. http://dx.doi.org/10.1680/geot.2008.3770.

Sun, D.-L., Rao, Q.-h., Wang, S.-Y., Yi, W., Shen, Q.-q., 2021. A new mixed-mode fracture criterion of anisotropic rock. Eng. Fract. Mech. 248, 107730. http://dx.doi.org/10.1016/j.engfracmech.2021.107730.

Taiebat, M., Dafalias, Y.F., 2008. SANISAND: Simple anisotropic sand plasticity model. Int. J. Numer. Anal. Methods Geomech. 32 (8), 915–948. http://dx.doi.org/10.1002/nag.651.

Tian, Y., Yao, Y.-P., 2017. A simple method to describe three-dimensional anisotropic failure of soils. Comput. Geotech. 92, 210–219. http://dx.doi.org/10.1016/j.compgeo.2017.08.004.

Tobita, Y., 1988. Yield condition of anisotropic granular materials. Soils Found. 28 (2), 113–126. http://dx.doi.org/10.3208/sandf1972.28.2_113.

Wan, R.G., Guo, J., 2001. Drained cyclic behavior of sand with fabric dependence. J. Eng. Mech. 127 (11), 1106–1116. http://dx.doi.org/10.1061/(ASCE)0733-9399(2001)127:11(1106).

Wang, H., Sun, H., Ge, X., Niu, F., 2023. An anisotropic failure criterion for cross-anisotropic soils. KSCE J. Civ. Eng. 27 (9), 3808–3823. http://dx.doi.org/10.1007/s12205-023-2253-8.

Wang, S., Zhong, Z., Liu, X., 2020. Development of an anisotropic nonlinear strength criterion for geomaterials based on SMP criterion. Int. J. Geomech. 20 (3), 04019183. http://dx.doi.org/10.1061/(ASCE)GM.1943-5622.0001588.

Weber, J., 1966. Recherches concernant le contraintes intergranulaires dans les milieux pulvérents; Applicationa La Rhéologie de Ces Milieux. Cah. Français Rhéol. 2, 161–170.

Wheeler, S.J., Näätänen, A., Karstunen, M., Lojander, M., 2011. An anisotropic elastoplastic model for soft clays. Can. Geotech. J. 40 (2), 403–418. http://dx.doi.org/10.1139/t02-119.

Xiao, Y., Liu, H., Yang, G., 2012. Formulation of cross-anisotropic failure criterion for granular material. Int. J. Geomech. 12 (2), 182–188. http://dx.doi.org/10.1061/(ASCE)GM.1943-5622.0000136.

Yang, Z., Liao, D., Xu, T., 2020. A hypoplastic model for granular soils incorporating anisotropic critical state theory. Int. J. Numer. Anal. Methods Geomech. 44 (6), 723–748. http://dx.doi.org/10.1002/nag.3025.

Yao, Y., Lu, D., Zhou, A., Zou, B., 2004. Generalized non-linear strength theory and transformed stress space. Sci. China Ser. E: Technol. Sci. 47 (6), 691–709. http://dx.doi.org/10.1360/04ye0199.

Yao, Y., Tian, Y., Gao, Z., 2017. Anisotropic UH model for soils based on a simple transformed stress method. Int. J. Numer. Anal. Methods Geomech. 41 (1), 54–78. http://dx.doi.org/10.1002/nag.2545.

Yao, Y.-P., Wang, N.-D., 2014. Transformed stress method for generalizing soil constitutive models. J. Eng. Mech. 140 (3), 614–629. http://dx.doi.org/10.1061/(ASCE)EM.1943-7889.0000685.

Yin, Z.-Y., Chang, C.S., Hicher, P.-Y., Karstunen, M., 2009. Micromechanical analysis of kinematic hardening in natural clay. Int. J. Plast. 25 (8), 1413–1435. http://dx.doi.org/10.1016/j.ijplas.2008.11.009.

Yin, Z.-Y., Zhao, J., Hicher, P.-Y., 2014. A micromechanics-based model for sand-silt mixtures. Int. J. Solids Struct. 51 (6), 1350–1363. http://dx.doi.org/10.1016/j.ijsolstr.2013.12.027.

Yoshimine, M., Ishihara, K., Vargas, W., 1998. Effects of principal stress direction and intermediate principal stress on undrained shear behavior of sand. Soils Found. 38 (3), 179–188. http://dx.doi.org/10.3208/sandf.38.3_179.

Yu, Q., Du, S., Zhu, Q., Lu, Y., Luo, Z., Yong, R., 2024. Micromechanical anisotropic damage approach for understanding localized behavior of brittle materials under tension. Comput. Geotech. 173, 106498. http://dx.doi.org/10.1016/j.compgeo.2024.106498.

Zhang, B., Deisman, N., Chalaturnyk, R., Boisvert, J., 2024. Numerical upscaling of anisotropic failure criteria in heterogeneous reservoirs. Eng. Geol. 331, 107455. http://dx.doi.org/10.1016/j.enggeo.2024.107455.

Zhao, L.-Y., Ren, L., Niu, F.-J., Lai, Y.-M., Zhu, Q.-Z., Shao, J.-F., 2023. Estimation of elastic properties and failure strength of layered rocks with a multi-scale damage approach. Int. J. Plast. 168, 103681. http://dx.doi.org/10.1016/j.ijplas.2023.103681.

Zhao, C., Salami, Y., Yin, Z.-Y., Hicher, P.-Y., 2017. A micromechanical model for unsaturated soils based on thermodynamics. In: Poromechanics VI. American Society of Civil Engineers, pp. 594–601. http://dx.doi.org/10.1061/9780784480779.073.